INVESTIGATION OF STRESSES IN ALUMINIUM A356 ALLOY PELTON TURBINE BUCKETS

RICHARD NJIHIA MBIU

MASTER OF SCIENCE

(Mechanical Engineering)

JOMO KENYATTA UNIVERSITY OF AGRICULTURE AND TECHNOLOGY

2021

Investigation of Stresses in Aluminium A356 Alloy Pelton Turbine Buckets

Richard Njihia Mbiu

A Thesis Submitted in Partial Fulfillment of the Requirements for the Degree of Master of Science in Mechanical Engineering of the Jomo Kenyatta University of Agriculture and Technology

2021

DECLARATION

This thesis is my original work and has not been presented for a degree in any other university.

Signature: ..... Date .....

Richard Njihia Mbiu

This thesis has been submitted for examination with our approval as the University Supervisors:

Signature: ..... Date .....

Prof. S. M. Maranga, PhD

JKUAT, Kenya

Signature: ..... Date .....

Dr. Eng. Hiram M. Ndiritu, PhD

JKUAT, Kenya

DEDICATION

I dedicate this work to my loving family.

ACKNOWLEDGEMENTS

I thank the Almighty God for giving me the opportunity to do this research. I also sincerely thank my supervisors Prof. S.M.Maranga and Dr. Eng. Hiram Ndiritu who guided and supported me throughout this research. I am also very grateful to JKUAT and JICA BRIGHT Project for funding this research.

I would like to thank the members of staff in the Department of Mechanical Engineering and Engineering workshops (JKUAT) for their assistance during the research work. Special gratitude goes to the Engineering Foundry workshops staff Mr. Mwai Mr. Muigai and Mr. Nyanjui for his invaluable counsel and encouragement during this research.

Finally, I extend my gratitude to my parents for the moral support that they gave me throughout the research period.

TABLE OF CONTENTS

LIST OF TABLES

LIST OF FIGURES

LIST OF ABBREVIATIONS

BRPB	Bolted Runner Pelton Bucket
CAD	Computer Aided Design
CAM	Computer Aided Manufacturing
CFD	Computational Fluid Dynamics
CNC	Computer Numerical Controlled
FEM	Finite Element Method
FVM	Finite Volume Method
JKUAT	Jomo Kenyatta University of Agriculture and Technology
PCD	Pitch Circle Diameter
SST	Shear Stress Transport

NOMENCLATURE

a_{jet}	Cross sectional area of the jet $[m^2]$
c	Linear velocity of the water jet [m/s]
C_p	Specific heat capacity
d_{jet}	Diameter of the jet [m]
E	Young's Modulus $[N/m^2]$
F	Pulse force [N]
g	Gravitational acceleration $[m/s^2]$
G	Shear Modulus [Pa]
H	Head [m]
m	Mass [kg]
$\dot{m}$	Mass flow rate [kg/s]
M_T	Torque $[N.m]$
p	Pressure [Pa]
P_{jet}	Kinetic power of the water jet [W]
P_T	Turbine power output [W]
Q	Flow rate $[m^3/s]$
T	Temperature $[^0]$
t	Temporal coordinates
u, v	Velocity components in x and y direction
x, y, z	Spacial coordinates

GREEK SYMBOLS

ρ	Density $[kg/m^3]$
u	Peripheral velocity of turbine runner [m/s]
ω	Rotational speed [rad/s]
η	Turbine efficiency
φ_n	Frictional loss coefficient
β	Bucket angle of setting $[^0]$
θ	Jet deflection angle $[^0]$
ε	Elastic strain
σ	Stress $[N/m^2]$
υ	Poisson's Ratio
μ	Dynamic viscosity
λ	Thermal conductivity $[W/m/K]$

ABSTRACT

Rapid increase in energy consumption and global warming threatening the environment together with the unpredictable increases of the fossil fuel prices has increased the importance of renewable energy sources. The need to reduce use of fossil fuel as energy sources in rural areas which are not connected to power grid is a major concern in order to stop a further decline in the environment. To replace this non-renewable energy many different alternative power sources are being researched on and implemented. Demand for rural electrification in the country has triggered use of small scale hydro turbines. Therefore, manufacturing of turbines using locally available materials such as recycled aluminium scrap metal has resulted. Effective performance of these turbines, turbine efficiency and dynamic behavior under different operating conditions need to be predicted. This research investigates the variation on ratio between the bucket width and the jet diameter on turbine performance. A decrease in the ratio leads to an increase in cyclic load and therefore an increase in stresses on the buckets and the turbine hub. This is a notable problem with bolted runner Pelton buckets. In addition to cyclic loading, corrosion aggravates stress concentrations around the bolts leading to turbine failure. This work sought to improve the profile of Pelton turbine buckets in order to optimize their performance. This was accomplished through design, manufacture and testing of improved models of the buckets. Design and production of the test Pelton buckets was done using Computer Aided Design (CAD) and Computer Aided Manufacturing (CAM) software. Investigation of forces and stresses on a Pelton buckets was done using structural analysis on commercial simulation software, ANSYS Structural. The simulation results were then validated with experimental results obtained from bending test conducted on the two buckets samples. The investigation indicated a 14% percentage reduction on the stresses developed on the buckets by introducing a ridge on the backside of the bucket that enabled even distribution of stresses on the bucket without compromise on the bucket width to jet diameter ratio. As a result, without altering the optimum bucket width in relation to water jet diameter a higher power output was achieved by optimizing the bucket profile.

CHAPTER ONE

INTRODUCTION

1.1 Background

The socio-economic development and increased living standards with the fast growing manufacturing industry has led to a major increase in electricity demand. Being the basic input of all kinds of economic activity, electrical energy has become an indispensable component of social life. Less than 20% of the total population and 5% of the rural population in Kenya has access to electricity. Although overall electric production has increased at 5% per year since 1980, consumption of electricity per capita has only increased at 1.2% per year (Kiplagat J. et al., 2011). This is as a result of the growing population and the inefficiencies that exist on the grid as well as the prohibitively high costs for infrastructure development. A significant increase in the country's energy supply is necessary in order to keep up with demand and continue to increase per capita electricity consumption. As an importer of petroleum fuels, Kenya spends close to 55% of foreign exchange to import oil (Kiplagat J. et al., 2011). On the other hand, there is a high dependence on wood biomass energy. This has exerted considerable pressure on the remaining forest and vegetation, thereby accelerating the processes of land degradation. Moreover, despite the abundance of potential and a strong growth in demand for electricity, the country faces constraints in satisfying electricity demand. Kenya's electricity power mix is among the most sustainable in the world, with 80% of electricity coming from renewable sources. However, a substantial proportion of renewable energy resources are unexploited. Of the potential renewable sources, Kenya has harnessed only about 30% of its hydropower sources, approximately 4% of the potential geothermal resources and much smaller proportions of proven wind and solar power potentials (Kiplagat J. et al., 2011).

Kenya's National Energy Policy is designed to facilitate provision of clean, sustain-

able, affordable, reliable and secure energy services at least cost while protecting the environment. The Kenyan government is using three policy tools to facilitate the adoption of renewable energy which are; to increase the country's energy supply, close the demand gap and ultimately enable economic growth. Renewable energy mini-grids powered by biomass gasifiers or small-hydro plants appear to be the favored option due to their lower levelised costs, provision of power, potential to provide a 24 hour service and ability to host larger capacity systems that can power a wide range of electricity uses (Yadoo A. et al., 2012).

Among potential renewable energy sources in Kenya including geothermal, biomass and small hydro, small hydro has emerged as an energy source which is accepted as renewable, easily developed, inexpensive and harmless to the environment. These features have increased small hydropower development in value giving rise to a new trend in renewable energy generation. Hydro power is considered clean source of energy that does not consume but only uses the water. After producing power the water is available for other purposes such as domestic use and agriculture (Jagdish L. 1975).

Small hydro units are compared to other decentralized renewable energy options such as geothermal, wind and solar are characterized by high initial capital costs which are offset to some extent by relative low operating costs. This means that 'entry costs' are likely to be beyond the reach of many rural people, even if the life cycle cost of these options is the lowest (Logan 2003). This calls for the reduction in the cost which would be achieved by lowering the cost of turbine, a key component of small hydro systems. Currently in Kenya small turbines are imported from India, Sri-lanka and China and the cost is high. Based on affordability, small turbines are forced to operate above optimum conditions in order to produce maximum power making them to fail under excessive water jet loading.

1.2 Pelton Turbine

Pelton turbines are classified as impulse turbines; where by water from a high head is passed through a small nozzle that converts the head to an atmospheric pressure jet of high velocity. The jet strikes the blades at one position as they pass by and imparts a momentum change due to the cyclic force on the buckets. The pressure of liquid does not change while flowing through the turbine rotor. The Pelton turbine is used to convert kinetic energy of water flow at a given head into mechanical energy. The transfer of the total energy occurs at atmospheric pressure unlike in reaction turbines whereby the water fills the blade passages and the head change or pressure drop occurs within the impeller. The pressure of liquid changes while it flows through the rotor of the machine. The change in fluid velocity and reduction in its pressure causes a reaction on the turbine blades. A water jet stemming from the nozzle impinges on the buckets (double hemispherical cups) located at the periphery of a wheel (hub) making it to rotate as shown in Figure 1.1. The jet strikes the buckets

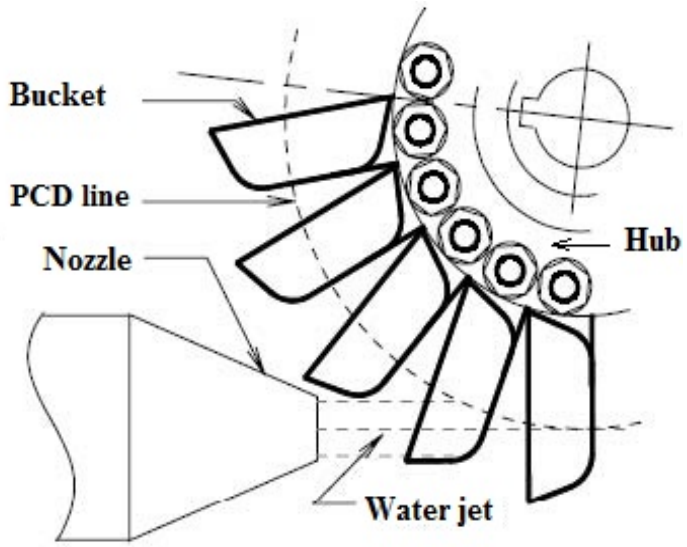

Figure 1.1: Pelton turbine

at the central dividing edge called a splitter. The water jet strikes the splitter symmetrically and is equally distributed into the two halves of hemispherical bucket as shown in Figure 1.2 (Helmut K et al., 2008).

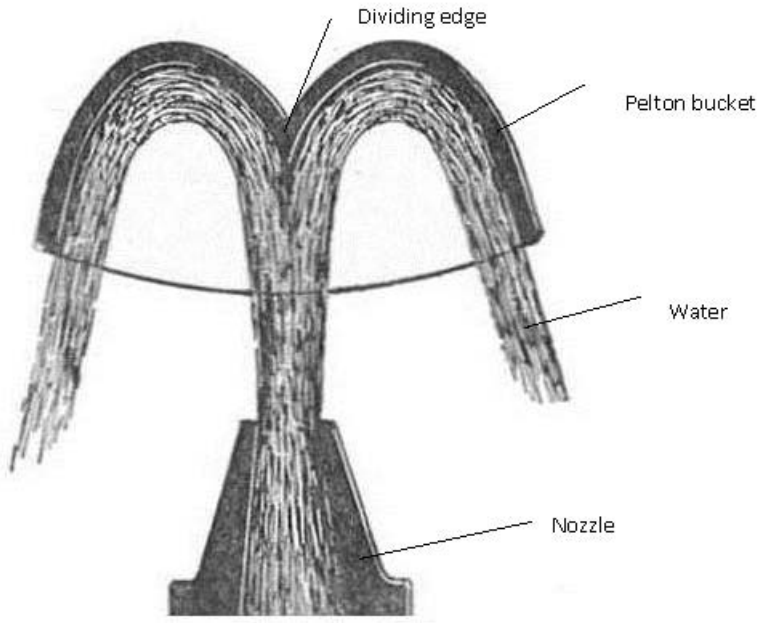

Figure 1.2: Water jet bucket interaction

1.3 Problem Statement

The demand for power in rural areas is a major concern even in areas near hydro potential sites. Most of the people in these places are characterized by low income. This limits them to afford the right size of turbine that will generate enough power that they require. As a result they buy small turbines and use them in extreme working conditions i.e higher operating head and flow rate than rated in order to generate more power. The turbine runner is overloaded and subjected to a combination of stresses caused by centrifugal force and cyclic loads. The centrifugal force is as a result of the mass of the fast rotating turbine runner. Cyclic loads are induced each time the bucket meets the water jet (Parkinson E. et al., 2007). On high-speed, the individual buckets undergo high repetitive forces as the turbine operates. Therefore, the runner is vulnerable to excessive loading failure. This is a major consideration in the design process and formed the bases of this research work. The cyclic overload induce excessive load on the bearings carrying the turbine runner and this is a common cause of bearing failure before the scheduled maintenance

period.

High demand of electricity in the rural areas is prompting local fabricators to develop hydro turbines that are not up to standard and consequently fail within a very short period of operation. In good production practice, high surface finish reduces hydraulic friction losses and as a result increases in power output. The method used to produce a turbine should also not introduce pre–induced stresses especially on the turbine blades since this would accelerate the failure rate. The material used in fabrication should be of high strength with good wear and corrosion resistance characteristics.

1.4 Objectives

The main objective of this study was to establish operating conditions of pelton wheel in order to optimize size and performance of the turbine developed from recycled aluminium A356 alloy. This was to be achieved through the following specific objectives.

(i) To design and construct standard buckets for a pelton wheel turbine using casting technique.

(ii) To investigate force and stress distribution on the turbine bucket.

(iii) To carry out structural analysis on a stationaly bucket to determine stresses developed on a stationary bucket under equivalent jet force.

(iv) To optimize the bucket width to jet diameter ratio for maximum power output within cyclic loading safety zone.

1.5 Significance of the Study

Limited knowledge on use of small hydro turbines have greatly hindered utilization of the many potential hydro power sites in urban centers in Kenya that are yet to

have electricity supply. Exponential industrial growth in Kenya has made it even more difficult to consider the rural population in electrification extension program. Appropriate production techniques of affordable and reliable power generation units to be used in isolated areas in Kenya need to be addressed.

This research will facilitate production and utilization of appropriate small hydro turbines using locally available material such as recycled aluminium scrap metal. To demonstrate on a cost effective and simple technology of hydro turbine production, casting was adopted which is appropriate in local manufacturing of small turbines to be used in hydro potential rural areas in Kenya.

During operation of Pelton turbines the massive number of applied cyclic forces by the water jet has been found to make cyclic failure the most likely failure mechanism. Investigation on the stresses developed on the buckets for different working conditions were carried out and optimum conditions for maximum power established for a 152 mm PCD size Pelton turbine. This gives confidence in utilizing this size of a Pelton turbine without fear of failure under cyclic forces.

1.6 Thesis Document Organization

The thesis is organized into 5 chapters and the current one is the introduction to this research which provides an enlightening on the existing problem and how Small Pelton turbines can be used to provide energy solutions. In chapter 2 numerical tools and experimental techniques are reviewed based on findings of researchers from which gaps are identified to justify the method applied in this study.

Chapter 3 presents the numerical calculations based on the empirical formulas and the experimental setups used in order to obtain the operating parameter and determine the optimum operating conditions for the Pelton turbine. In chapter 4, the stress analysis results obtained are presented and comparison made between the modeling results and experimental results. Chapter 5 contains the conclusions on the optimum power output for a 152 mm PCD Pelton turbine and recommendations

for further work. The references cited in the thesis and the appendices are presented thereafter.

CHAPTER TWO

LITERATURE REVIEW

2.1 Overview

A review of different methods used to improve the Pelton turbine efficiency and power output are presented in this chapter. Previous research consists mainly of numerical, experimental and analytical studies. This ranges from Pelton bucket profile optimization, flow analysis, studies on force redistribution on the bucket, analysis on stress distribution on the bucket, nozzle and casing modification and computer simulations to maximize operating conditions. The sections that follow briefly highlight previous research work with attention focused on key aspects analysis relevant to the Pelton turbine power output optimization. Arising gaps and challenges in each research work were identified and used as guidelines in developing this research.

2.2 Pelton Turbine Use in Power Generation

Water turbines are means of extracting energy from falling water. Different types of turbines work under different operating conditions in terms of head and flow. Pelton turbine has been in use for more than 100 years effectively over a relatively wide range of flow conditions and are relatively small in size compared to reaction turbines of the same capacity. The design of Pelton runner was patented in 1880 by Lester Allen Pelton and notable technological changes have taken place from forged runner to separate cast buckets (Gaurangkumar C. et al., 2005). Pelton turbines work best under conditions of high head and low flow. This means they can utilize high heads to produce a lot of power for a small unit. Pelton turbines are also reasonably easy to make. A given turbine can be used for a range of heads and flows; unlike Propeller or Francis turbines, the runner does not have to be designed for specific flow conditions. The runner has space around it, making it much easier to inspect the blades and work on them unlike most of the other turbine. Even at modest heads, small Pelton wheels can be made to run at high speed which allows them to be matched to

generators without the need for belt drive or gearbox to change the speed. In many cases the Pelton turbine is mounted on the generator shaft, so that the turbine does not need its own shaft or bearings. Such a layout greatly simplifies the installation and is cheap. Common use for Pelton turbine have been for small, self-contained generating units of a few kilowatts, often called peltric sets. Although electricity generation is the most common use of Pelton turbines, the mechanical power can be used to drive any rotating machinery: crop-processing, saw mill and woodworking, irrigation pumps, potteries, mechanical workshop equipments, food processing etc. By modifying the bucket profile of a Pelton bucket, significant improvement on the power output without much effect on the turbine operation is possible (Kovalev N. 1961).

2.3 Numerical Models

The flow in Pelton turbines are considered to be unsteady due to periodic change of the relative position between the water jet and the bucket (Kuhlmann H. 1998). The flow is also three dimensional and turbulent influenced by the rotation-induced forces of the water jet onto the bucket. In preparation for the structural analysis, an understanding on fluid flow on Pelton bucket was needed. This section reviews different research work on fluid flow modeling. The models were used to predict power output of hydro turbines by computational simulation aiming at reducing the time required at the design phase. Various developments on computational simulation for water turbines have already led to substantial improvement in the design and performance of hydro turbines (Sick M. et al., 2000). The subsections that follow highlight on some of the computational research work related to Pelton turbine.

2.3.1 Fluid Dynamic Analysis

Different computer simulations have been conducted by different researchers in order to study the flow behavior in hydro turbines. One is Computational Fluid Dynamics

(CFD) which is a computer-based method mainly used for simulating the behavior of systems involving fluid flow and heat transfer processes. It works by solving the equations of fluid flow over a region of interest, with specified known conditions on the boundary of that region. To study the flow behavior on Pelton buckets, (Helmut K et al., 2008) used a commercial CFD program called ANSYS FLUENT. The program was well suited to model complex internal flow. It has advanced meshing features and Finite Volume Method (FVM) that were easily interlinked with stress, thermal and dynamic analysis. FVM produced design data quickly and was able to help identify if a newly designed structure would work or not. This provided a guide on where the design needed to be modified. The method was used as a replacement of the hydraulic test rig modeling (Mack R. et al., 2006). The results presented did not link the flow behavior with the forces generated on the buckets which are of interest in this research. However, the CFD simulations results gave a better physical understanding of the pressure distribution on the inner surface of the bucket. This formed the basis for analysis forces and stresses that result by further carrying out structural analysis. Another method reviewed by (Mack R. et al., 2006) was Multi-Fluid Flow Modeling (MFFM) as highlighted below.

2.3.2 Multi-Fluid Flow Modeling

The multi-fluid model, also known as Mixture Model or 2-Phase Homogeneous Model was used in complex free-surface flow modeling thus very appropriate to use on Pelton buckets (Sick M. et al., 2000). This method works by solving the Navier-Stokes equations on a fixed grid through numerical diffusion. The numerical diffusion became severe especially when the deformation of the free surface was large and complicated. Mesh-free approaches have become increasingly popular to overcome this problem. Among them, the methods based on fully Lagrangian particle approaches appear promising. Kuhlmann and Ruth (Kuhlmann H. 1998) used the 2-Phase Homogeneous and the 2-Fluid Models to simulate the operation of the test turbine runner section at a given test head range. The obtained results were in form of

pressure distribution, water film thickness and flow patterns in the buckets.

Meshes composed of tetrahedral, hexahedral, and pyramidal elements were used in the simulations for results verification purpose. The computational domain was divided into 2 sub-domains, i.e. a stator with a dummy nozzle and a rotor with the runner, linked with a transient rotor-stator sliding interface. By assuming periodic flow, half of the runner was simulated as shown in Figure 2.1. For the boundary conditions, the incoming jet was assumed to be ideal, with a constant velocity profile determined from the specific energy and discharge conditions. The flow relative to the splitter was considered to be symmetrical. Turbulence was taken into account using a shear-stress model in order to account for the high shear stresses on the splitter sides (Perrig A et al., 2006). Initial conditions assumed a uniform velocity of 0 m/s which was imposed in the whole test turbine section, with the same turbulence data (Alexandre P. et al., 2005). This method was reviewed in the present study in order to have a clear understanding of pressure distribution and water flow patterns on the inner surface of the Pelton buckets. The review acted as a guide when determining the loading points on the bucket when carrying out stress analysis. Assumption made were that of the fluid flow pattern to have no turbulence and use of a section model of the turbine instead of the entire turbine runner. The two reviewed method were of great help in understanding the input conditions used to carry out the stress analysis on the Pelton buckets.

2.3.3 Case Study on Pelton Turbine Casing

In attempt to increase turbine efficiency of an already installed turbine, (Vesely J. et al., 2000) refurbished a 62.5 MW Pelton turbine casing and its nozzles. An increase of 14% in power output and efficiency increases by 1.4% with the new power output standing at 68.2 MW was attained. The power and efficiency improvement of the turbine were achieved by introducing a straight flow nozzle tips and by enlargement the turbine casing, creating more space on the turbine housing as shown in Figure

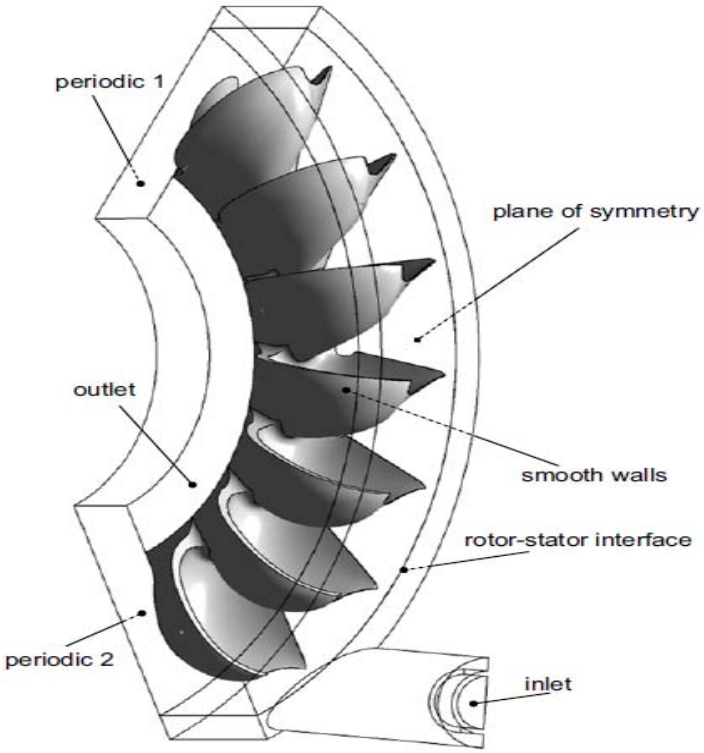

Figure 2.1: CFD simulations setup

2.2. The commercial CFD software Fluent was used for the flow simulations through the other parts of rehabilitated turbine. They showed that the casing has great effect

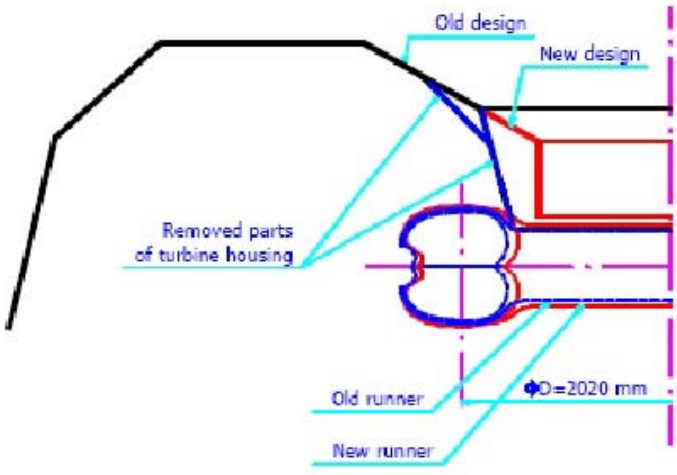

Figure 2.2: Turbine housing modifications

on the operation of a Pelton turbine and so it is important to include the casing as a factor in all investigations on power output. Since the work was done on an already installed turbine, modification of the casing to accommodate the new nozzle required refabricating the casing in order to fit the new nozzle in constrained area that had been already designed for the previous nozzle. The finite element software are costly in terms of license. Also very little modification in terms of design change could be done on already installed turbine.

A similar study on the shape of the casing was carried out as review in a subsection in the next section.

2.4 Experimental Studies

Experimental reviews on investigations of performance improvement are presented in this section. Different experimental methods used on Pelton turbines in attempt to increase turbine efficiency and power output are highlighted.

2.4.1 Force Redistribution on Pelton Buckets

Mayse F. et al., 2002 developed a design of Pelton wheel called hooped pelton turbine as shown in Figure 2.3 (Bernard M. et al., 2003). The design was based on water jet force redistribution on the turbine runner. In a typical Pelton runner, the buckets are encased onto a central rim in case of a one piece runner or mechanically bolted in case of separated buckets. The researchers tried to minimize these effects by adding two hoops on either set of buckets as shown in Figure 2.3, allowing stresses to be more efficiently distributed all round the runner.

The whole structure withstands the jets loads, although the hoops contribute to extract material cost and this method was proved to be effective. Stress results were analyzed in terms of maximum stress range over time at any point of the structure of the hoops and compared to fatigue limits of the runner material. The design of the bucket ensures conversion of jet force into tangential force that eventually causes

Figure 2.3: Hooped Pelton turbine runner

rotation. However, during this conversion shear and bending forces were induced at the regions where buckets were mounted to the turbine ring. The attachment zone is subjected to cyclic high bending stresses as the bucket repeatedly passes into the jets. The bucket experiences vibration due to repeated loading since it is mounted as a cantilever onto a disc. If not properly designed or manufactured, resonance may occur and severely increase the dynamic stress causing failure.

2.4.2 Stress Analysis on Hooped Pelton Wheel

Channiwala S. et al., 2008 studied flow analysis on a typical Pelton wheel and compared the results with those of a hooped Pelton turbine. The aim was to show the stress distribution in the turbine runner. At internal and external radius of buckets, the percentage reduction of Von Mises stresses on a typical Pelton wheel, single hooped Pelton wheel and a double hooped Pelton wheel were compared. It was found that the power developed and efficiency in a hooped runner was slightly higher than in a typical runner. It showed a good hydraulic behavior of the hooped Pelton runner.This was attributed to improved runner design that caused even force distribution thereby reducing vibrations. The hoops allowed stresses to be minimized and distributed more efficiently on the buckets. Additional cost of turbine was incurred by introducing the hoops and there was need to seek for a simple way of

addressing this without compromising on stress distribution on the turbine runner. To overcome this, ridges were introduced in this research work and stress analysis results compared with those of buckets without the ridges.

2.4.3 Study on Jet/bucket Flow Interactions

Alexandre et al.,2005 conducted a series of practical experiments on the flow parameters in a Pelton turbine. They deduced that the impact pressure on the bucket strongly depends on the energy coefficient, that is, the potential and kinetic energy in the water jet, the angle of impact and the initial jet/bucket interaction that causes the turning moment. The influence on the bucket torque and power was considered at the stage of performing mechanical test on the bucket. When a jet impacts the bucket inner surface, a high-pressure pulse, larger than the stagnation pressure was generated. This was caused by compressible effects of the water jet. The bucket backside acted as the suction side of this pressure undergoing the "Coanda effect". This generated a lift force contributing positively to the bucket and runner torques. This study demonstrated the three dimensional unsteady free surface flows in the buckets, However, it requires a complex fluid flow analysis equipment and laboratory.

2.4.4 Turbine Casings Shapes and Effects of the Splashed Water

Heinz B. et al.1997 estimated the influence of the splashed water distribution in the casing on the turbine efficiency. The tests were made on 9 different casings. Figure 2.4 shows one of the casings with cylindrical dome. The radius R_g and the width of the dome were varied and different results compared. Figure 2.5 shows an example of a tested casing with a rectangular dome. Modifications were made on the width of the dome. For a constant position of the needle of the nozzle and a constant head (constant unit discharge) the best efficiency point and the corresponding unit speed was located. Minimum water slashing was attributed to improved efficiency and the corresponding unit power output.

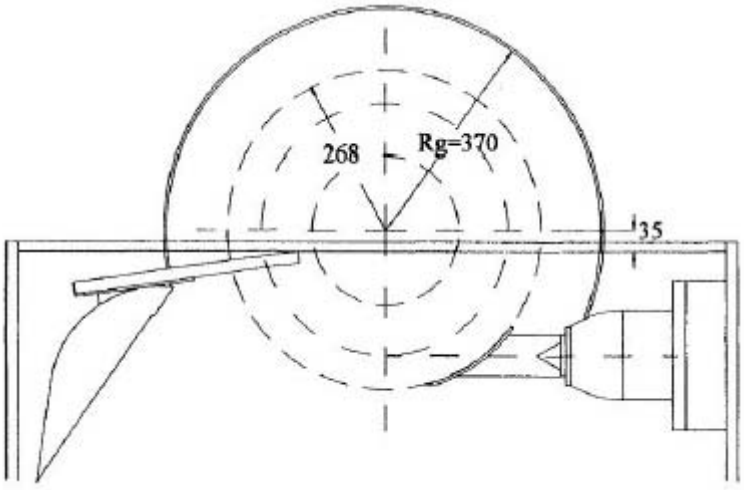

Figure 2.4: Turbine casings with cylindrical dome

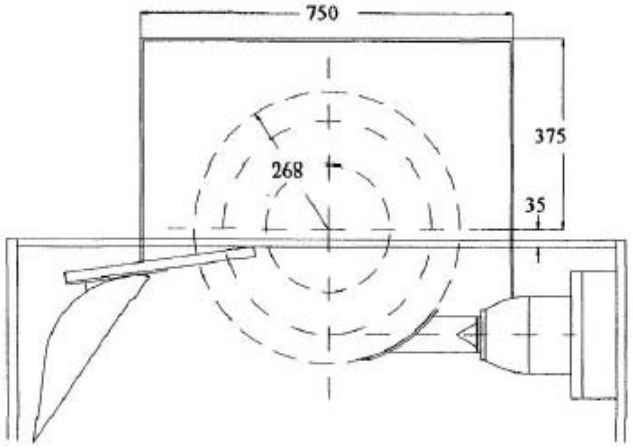

Figure 2.5: Turbine casing with a rectangular dome

The challenge was that to maintain a constant discharge, automatic adjustment of the position of the needle was required that needed continuous monitoring of the flow pattern to give a constant turbine speed.

2.4.5 Pressure Measurements using Piezo-electric Sensors

Kvicinsky S. et al., (2002) performed pressure measurements in non-rotating Pelton buckets in steady state to validate numerical simulations. The first measurement of the unsteady pressure in a rotating bucket was carried out by Avellan et al., 2006

where 3 piezo-electric pressure sensors were installed on a bucket and pressure results recorded on introducing the water jet. They fitted a reduced scale Pelton runner with 32 flush-mounted unsteady pressure sensors, providing the first set of unsteady pressure measurement in a runner under normal operating conditions. According to the shape of the measured signals, 5 zones were defined on the bucket inner surface The results showed that zones that are reached at the beginning of the cycle are better predicted than the zones reached by the flow at the end of the cycle. The amplitudes became underestimated, while the timing remain in good accordance with the measurements. Another challenge was that the pressure on the backside was poorly simulated and the measured data was far from the empirically calculated data. Also no pressure sensor was mounted directly in the tip, a theoretical approach need to be carried out to estimate the pressure amplitudes during the initial impact. Longatte F. et al., 1999 recommended that a kinematic study need to be performed to determine the local speeds and angles of attack at the instant of impact and the transient pressure amplitudes to be estimated using a simplified hydroacoustic model. In this research the jet force was numerically calculated given the fact that use of Piezo-electric Sensors was a costly process and high precision recording data loggers and high resolution camera were difficult to obtain.

2.4.6 Pressure Distribution Test Rigs

Zhang Z. et al., (2007) developed a test rig for the measurement of the pressure inside the buckets. A schematic diagram of a test rig is shown in Figure 2.6. The test rig consisted of a pressure pump to provided the desired head and a flow rate. The fluctuations in the flow was absorbed by pressure tank. Pressure was monitored outside the pressure tank and entrance of nozzle through the pressure gauge.

The pressure was measured in grid points of the inner surface of the bucket. The pressure intakes were placed at the points of a regular orthogonal network; i.e. x-axis spacing and the y-axis. Copper taps were then connected with flexible trans-

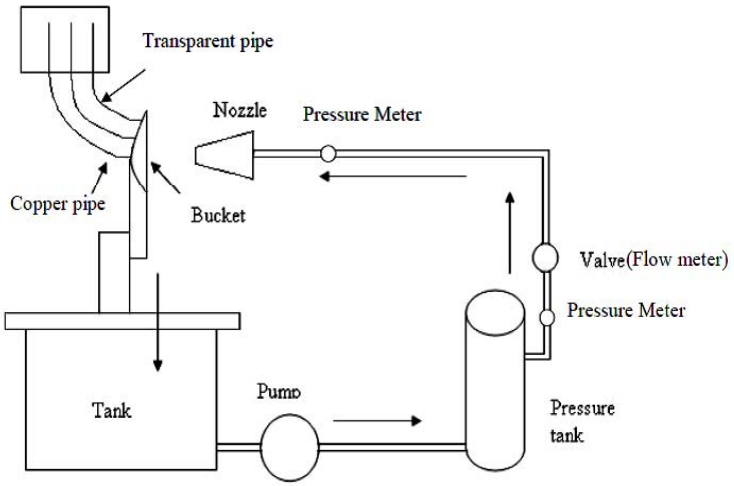

Figure 2.6: Pressure distribution test rig

parent PVC pipes for water column reading. The bucket was fixed onto the test rig upstream of the jet in a fixed member. The pipes were fixed in the board and calibrated to monitor total pressure at different points on the bucket. The water column height in each pipe was recorded. The pressure was measured inside the bucket profile with three different incidence angles i.e. 0^o (bucket was fixed normal to the jet), $+15^o$(bucket was in an inclined position away from the jet) and -15^o (bucket was in an inclined position towards the jet) with respect to the nozzle. The height of water column from the reference point of nozzle axis was measured and recorded as pressure head at different points. This was an appropriate way of measuring pressure distribution on the inner bucket surface. The result were in line with numerical calculation and this affirmed the use of numerical modeling in this research.

2.5 Analytical Studies

2.5.1 Turbine Selection Charts

Simplified charts have been developed to aid in selection of turbines especially for small scale plants. A sample of such Pelton turbine data chart is show in Figure

2.7. The precise theoretical analysis of Pelton turbines has been said to be more difficult due to complexity of the flow, thus the need for flow simulation technique application (Logan 2003).

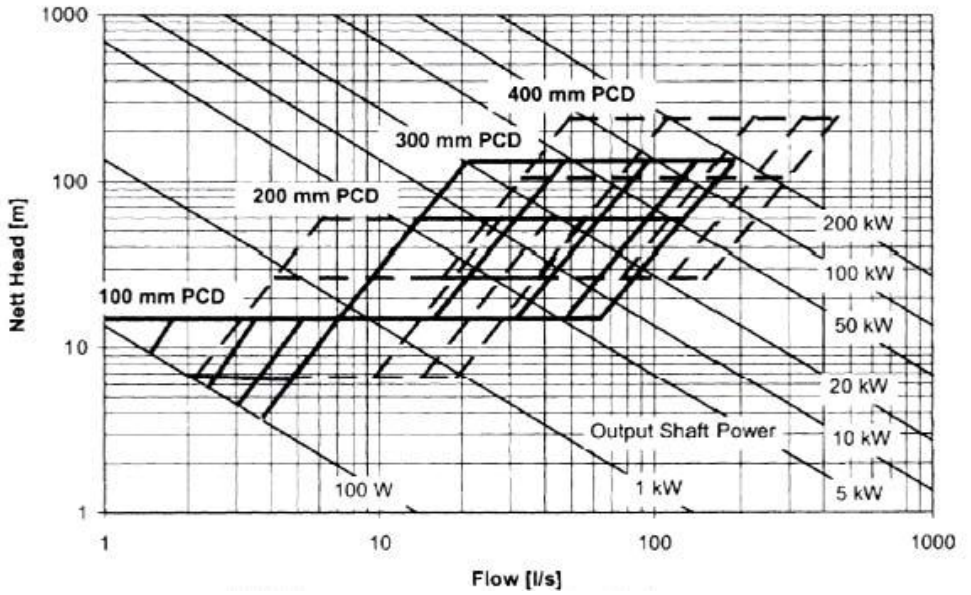

Figure 2.7: Pelton turbine range for various sizes of PCD

2.5.2 Turbine Comparison using Hill Charts

Ciocan G. et al., 2007, presented a technology that accelerated the development of hydro turbines by fully automating the initial testing process of prototype turbine models and automatically converting the acquired data into efficiency hill charts that allow straight forward comparison of prototypes performance. They illustrated testing procedure of both reaction and impulse turbines using models of Francis and Pelton turbines respectively. These hill charts can then be used in research and development to quickly evaluate and compare the performance of initial turbine prototype designs before proceeding to much lengthier and more expensive development stage of the chosen design. The acquired data was processed into meaningful results of the standard form. Moreover, if the model dimensions and the test conditions are in agreement with the limits provided in the testing standard, scaling can be done

for industrial hydropower plant designing. There are challenges in developing an appropriate hill chart by fully automated test, the process is time consuming and requires a fast processing computer for more accuracy.

2.5.3 Performance Prediction using Dynamic Flow Pattern

Xiao Y. et al., (2007) predicted the dynamic performance on pelton turbine through the dynamic energy efficiency of the bucket and power efficiency of the bucket was predicted from the dynamic flow pattern of the free-surface sheet flow in the rotating bucket. The dynamic discharge efficiency of bucket was defined as the resident discharge in the bucket at the respective moment. The hydraulic performance of Pelton turbine was dynamic due to the unsteady flow in the rotating buckets in time and space. The fundamental equations of dynamic hydraulic performance was derived for the Pelton turbine under the single jet operation through the flow analysis based on the animated-cartoon frame method. As a result, parameters of the dynamic performance prediction at various unit speed under the optimum needle stroke were obtained. However, the method is not applicable for multi-nozzle Pelton turbines where jet interference are inevitable.

2.6 Summary of the Gaps

Small Pelton turbines are applicable to generate power above the manufactures rating in most hydro potential areas and still operate within a safety region without breakdown failure due to over loading. They have also emerged as an energy source which are accepted as renewable energy, easy to develop, inexpensive and have no negative impact on the environment. Various methods have been deployed to improve on the power output and below is a summary of the shortcomings of the current improvement methods.

(i) Most methods tend to improve on efficiency and power output of the turbine without focusing on the safety operation range or the maximum limits

conditions that the turbine can be operated without failure.

(ii) There is limited improvement in terms of the turbine runner and casing that can be done on existing/ installed turbine in order to change the power output of the turbine.

(iii) Studies on flow patterns do not give the optimal operating conditions of the turbine and in the reviewed case the improvement of the power output was below 2%.

(iv) From the existing turbine selection charts, it is not possible to determine or predict the performances of the turbine at a given operating condition, thus it is difficult to estimate the service life or the rupture threshold due to fatigue stresses experienced by the turbine.

This research narrows down to study the main component of Pelton turbine which is the buckets. The research simulates and obtains the optimal conditions for maximum power generation on one bucket, eliminating the need to simulate the entire turbine given the complexity of the Pelton turbine buckets which will be more time-consuming and computationally expensive. A further step was taken to incorporate the previous works on flow studies with structural behavior of Pelton buckets made from aluminium A356 alloy. As a result this work will give confidence in utilization of the studied Pelton turbine size without fear of failure under cyclic forces.

CHAPTER THREE

METHODOLOGY

3.1 Background

The problem of developing a reliable method for predicting the optimum operating conditions of a Pelton turbine has been in existence for a long time. The need for more power from a turbine by operating it above the specified conditions leads to excessive loading causing the turbine to fail under stress loading. In this research, forces on the turbine buckets were calculated and used to generate through simulation and experiments the equivalent stresses that cause these failures. Optimum operating conditions in terms of Head, Nozzle diameter, Flow rates and Power output are presented thereafter.

3.2 Numerical Modeling

In the following sections, numerical modeling on the Pelton buckets is explained in details. Formulas used in numerical calculation of the Pelton turbine parameters like the turbine efficiency, nozzle efficiency, turbine power output, jet force and jet velocities are presented here. Optimization was based on potential head and nozzle diameter variation. This was done in order to get the equivalent force impacting on the inner surface of the buckets. The results of forces from the numerical calculations were used as input conditions to do the structural analysis using ANSYS software. Stresses developed on the buckets were obtained. To validate the results, bending experiments were carried out on bending testing machine.

3.2.1 Numerical Calculations

Calculations based on the empirical formulas of Pelton turbines as highlighted in this chapter were done in order to obtain the operating parameter and determine the optimum operating conditions for a 152 mm Pitch circle diameter Pelton turbine. Then the head and the nozzle diameter parameters were varied in order to increase

the turbine power output and the jet loading on the buckets monitored (Brekke H. 1984). Investigations were done for power output between 1 kW and 10 kW.

3.2.2 Pelton Turbine Parameters

Turbine operating head, jet pressure and jet velocity were calculated with the assumption that the vane of a Pelton turbine did not move, the only effect was to reverse the jet direction. Apart from some energy lost to friction which was catered for by introducing bucket efficiency φ_b. The energy of the jet, and the magnitude of its velocity, remained the same. The water jet from the nozzle produces the kinetic energy that drives the turbine runner.

The velocity of the jet is assumed to be slightly reduced by the friction losses in the nozzles expressed by the friction loss coefficient φ_n (0.96-0.99 for polished surfaces and well designed nozzle shapes). The jet velocity c_0 was obtained from

$$c_0 = \varphi_n . \sqrt{2.g.H} = \varphi_n . \sqrt{\frac{2.p}{\rho}} \tag{3.1}$$

a function of head H or pressure p and it is generally assumed that $c_1 = c_0$ i.e the inlet velocity at the runner equals the jet velocity at the nozzle. Shaft power of the Pelton runner was calculated assuming an empirical value of deflection of the jet of $\theta = 165^0$. This axial component of the reflected jet was necessary to prevent the deflected water from hitting the following buckets on the runner.

$$P_T = M_T.\omega = F.u = \rho.Q.\left(1 - \cos\theta\right).\left(c_1 - u\right).u \tag{3.2}$$

The efficiency of a Pelton turbine η was then calculated from the following equations

$$\eta = \frac{P_T}{P_{jet}} = \frac{\rho.Q.\left(1 - \cos\theta\right).\left(c_1 - u\right).u}{\frac{1}{2}.\rho.Q.c_1^2} \tag{3.3}$$

and this equation was simplified by introducing a ratio k:

$$\eta = \frac{2.\left(1-\cos\theta\right).\left(c_1-u\right).u}{c_1^2} \tag{3.4}$$

$$\eta = 2.\left(1-\cos\theta\right).\left(c_1-k\right).k \tag{3.5}$$

This showed how the efficiency η depends on the ratio $k = u/c_1$.

With the first derivative set to zero, the value of k for maximum efficiency was obtained as

$$k\left(\eta_{max}\right) = 0.5 = \frac{u}{c_1} \tag{3.6}$$

For maximum efficiency the runner tip speed u was equal to half the jet velocity c_1. This was compared with maximum theoretical efficiency which is expressed as

$$\eta_{max} = \frac{1}{2}.\varphi_n^2.\left(1-\varphi_b.\cos\beta_2\right) \tag{3.7}$$

Theoretical efficiency was in the range of 0.95 for optimal values of the nozzle efficiency φ_n. Well designed Peltons reach an efficiency of 88-91% when they operate at 60-80% of full design flow (Thake J .2011).

3.2.3 Pressure and Head

Pressure just before reaching the nozzle was calculated by multiplying the head with the water density and the gravitational acceleration as shown

$$p = H.g.\rho \tag{3.8}$$

3.2.4 Pelton Nozzle Efficiency

The speed of the turbine N runner at pitch circle diameter (PCD) was calculated by using the formula

$$u = \omega.PCD/2 \tag{3.9}$$

with

$$\omega = 2.\pi.N/60$$

Whereas the speed of the jet c_1 was obtained from

$$Q = \dot{V} = c_1.a_{jet} \tag{3.10}$$

with

$$a_{jet} = \pi.\frac{d_{jet}^2}{4}$$

$$c_1 = \frac{Q}{a_{jet}} = \frac{4.Q}{\pi.d_{jet}^2}$$

Nozzle efficiency was obtained by dividing the kinetic energy of the jet by the hydraulic energy from the pressure.

$$\varphi_{nozzle} = \frac{\frac{1}{2}\rho Q c_1^2}{pQ} = \frac{\rho c_1^2}{2p} \tag{3.11}$$

Where ρ is density of the fluid, c_1 is the jet velocity, Q is the flowrate and p is fluid pressure.

3.2.5 Hydraulic Power

Assuming the absence of friction losses the water jet Power P_{jet} from the nozzle was obtained from

$$P_{jet} = \frac{1}{2}\dot{m}c_1^2 \tag{3.12}$$

Kinetic energy of jet flow equals hydraulic power of the water flow

$$= p.\dot{V} = p.Q$$

and

$$Q = \dot{V} = \frac{\dot{m}}{\rho}$$

thus

$$P_H = H.g.\dot{m} \tag{3.13}$$

where the power P_H of the falling water is expressed as

$$P_H = Q.\rho.g.H$$

Where ρ is density of the fluid, g is acceleration due to gravity, Q is the flowrate and H is the net head.

3.3 Stress Calculation

The main interest in calculating stresses on the stem of the bucket was to analyse the two load cases that cause the bucket to break off. The first was the runaway, which occurred when the external load was removed from the turbine and the runner accelerated to a high speed. This produced a large centrifugal force in the buckets, which snapped the stem of the bucket. The second case was the fatigue load caused by bending stress on the stem due to the water hitting the bucket every time it passes the nozzle. The main cause of failure was the fatigue load. The runaway load was easier to address by introducing a clamping mechanism on the stem of the bucket as shown in Figure 3.1 and thus the focus was on the fatigue load analysis.

3.3.1 Fatigue Load

The main fatigue load on a bucket came from the jet force. This created a bending stress in the stem every time a bucket passed the jet. Most turbines exceed one million bending cycles on the bucket within the first few weeks of operation (Thake J .2011). The point at which the worst fatigue stress occurred depended on how the buckets were fixed. In this case a single piece casting as shown in Figure 3.2, the maximum bending moment occurred at the section where each bucket joins the disk. This gave a maximum tensile bending stress at point 'x'. The jet force was

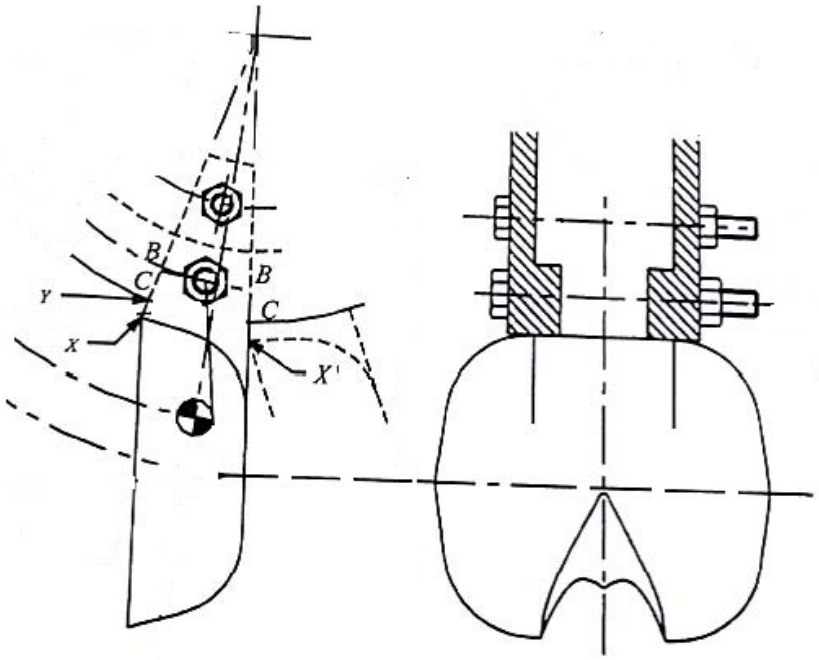

Figure 3.1: Clamped bucket to overcome runaway load

drawn for the maximum bending moment position, and had an effective moment arm about the neutral axis. The section modulus Z for the rectangular section of the bucket root was used and stress calculated according to Equation 3.14.

$$\sigma_f = \frac{M}{Z} = \frac{F_{jet}.a_{jet}}{Z} \tag{3.14}$$

Where;

σ_f is fatigue stress in the stem (N/mm^2)

M is bending moment $(N.mm)$

Z is stem section modulus= $\frac{I}{y_{max}}(mm)$

F_{jet} is jet force on bucket (N)

a_{jet} is moment arm from jet to section A-A (m)

D is runner PCD (mm)

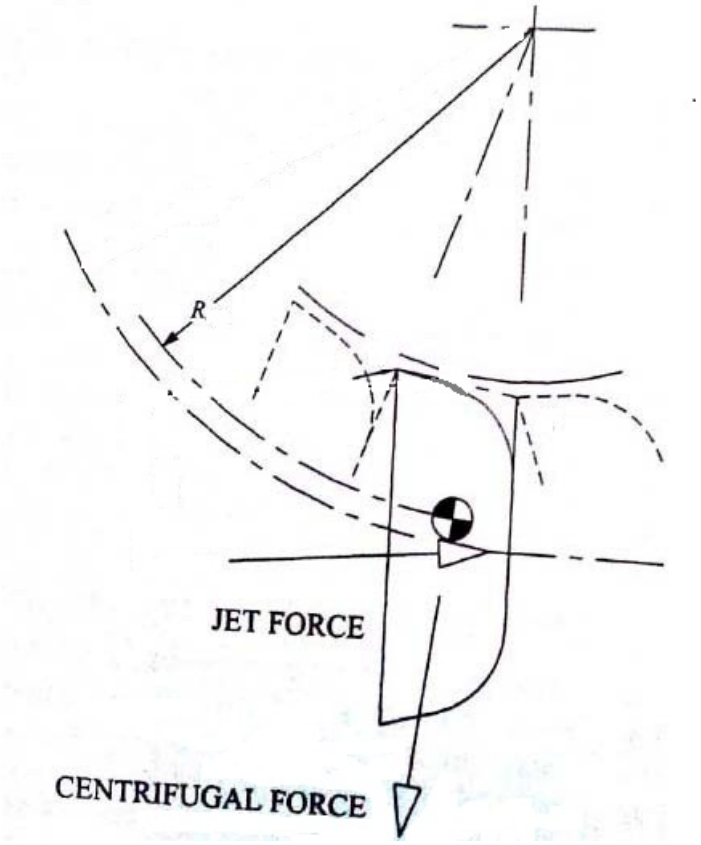

Figure 3.2: Forces on a Pelton bucket

The jet force was calculated from:

$$F_{jet} = \rho_w . Q_{jet} . C_v . \sqrt{2g . H_n} . (1 - x)^2 . (1 + \varsigma . \cos\gamma) \tag{3.15}$$

Where;

ρ_w is density of water=1000 (kg/m^3)

$Q_{jet}$is flow rate from one nozzle (m^3/s)

C_v is nozzle coefficient of velocity

g is acceleration due to gravity (m/s^2)

H_n is net head (m)

x is ratio of bucket velocity to jet velocity

ς is efficiency factor for flow in bucket

γ is outlet angle of bucket sides

At optimum operation speed, x was taken to be 0.46. γ was 15^0, C_v was taken as 0.97, and ς as 0.95.

3.4 Pelton Turbine Selection

Figure 3.3 shows alternative way of Pelton turbine sizing by use of approximate range of head and flow from charts. The diagonal lines show the shaft output power of the turbines. This charts used to guide on initial sizing of a turbine. Then the size of the runner and the number and the size of the water jets was determined from the equations below. The first consideration was the flow. The speed of the

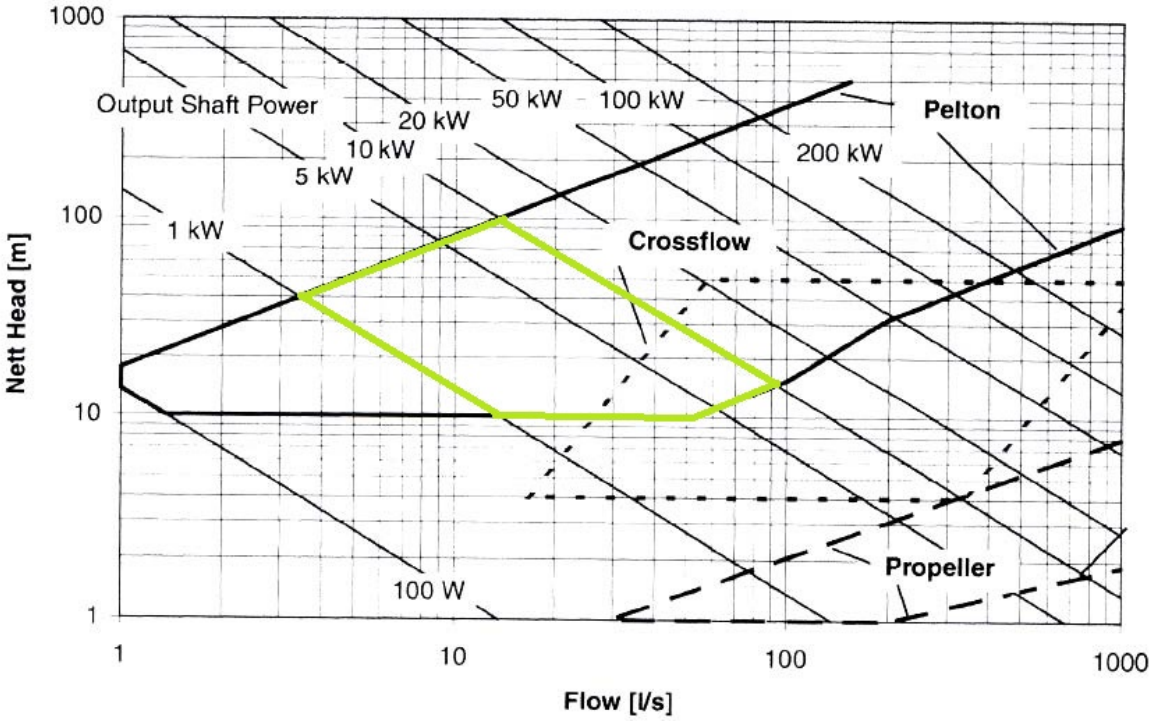

Figure 3.3: Range for different types of small-scale turbines [?]

water in the jet was dependent only on the head, and the flow was determined by

the speed, the area and the number of jets. Velocity of the jet was given by:

$$V_{jet} = C_v.\sqrt{2g.H_n} \tag{3.16}$$

The flow was obtained by multiplying the velocity by the cross-sectional area

$$Q = A_{jet}.V_{jet}.n_{jet} = \frac{\Pi.d_{jet}^2}{4}.V_{jet}.n_{jet} \tag{3.17}$$

Combining these gives

$$d_{jet} = \sqrt{\frac{4}{\Pi.C_v.\sqrt{2g}}}.\frac{1}{H_n^{\frac{1}{4}}}.\sqrt{\frac{Q}{n_{jet}}} \tag{3.18}$$

Using a C_v of 0.97

$$d_{jet} = \frac{0.54}{H_n^{\frac{1}{4}}}.\sqrt{\frac{Q}{n_{jet}}} \tag{3.19}$$

The dimensions of the bucket based on empirical relations for a 152 mm PCD Pelton turbine were obtained as length of 2.3 times the diameter of the jet, a width of 2.8 times the diameter of the jet, and a depth of 0.6 times the diameter of the jet. The angular deflection of the jet was 165^o and the bucket angle of setting 15^0.

3.5 Modeling

Solid modeling was used to develop the models for finite element analysis used in ANSYS structural analysis and to produce the machining data for pattern production. This was done using Autodesk Inventor software and the solid models are illustrated in Figure 3.4. The Figure shows the front and the back sides of the two Computer Aided Design solid models used in the analysis. The development of parameterized design data in the form of Computer Aided Design (CAD) solid models for the bucket was then imported to the ANSYS software and a block-structured grid generated and analyzed. The deformation and stress simulations on the buckets

were performed and results obtained compared with the experimental results in the next chapter.

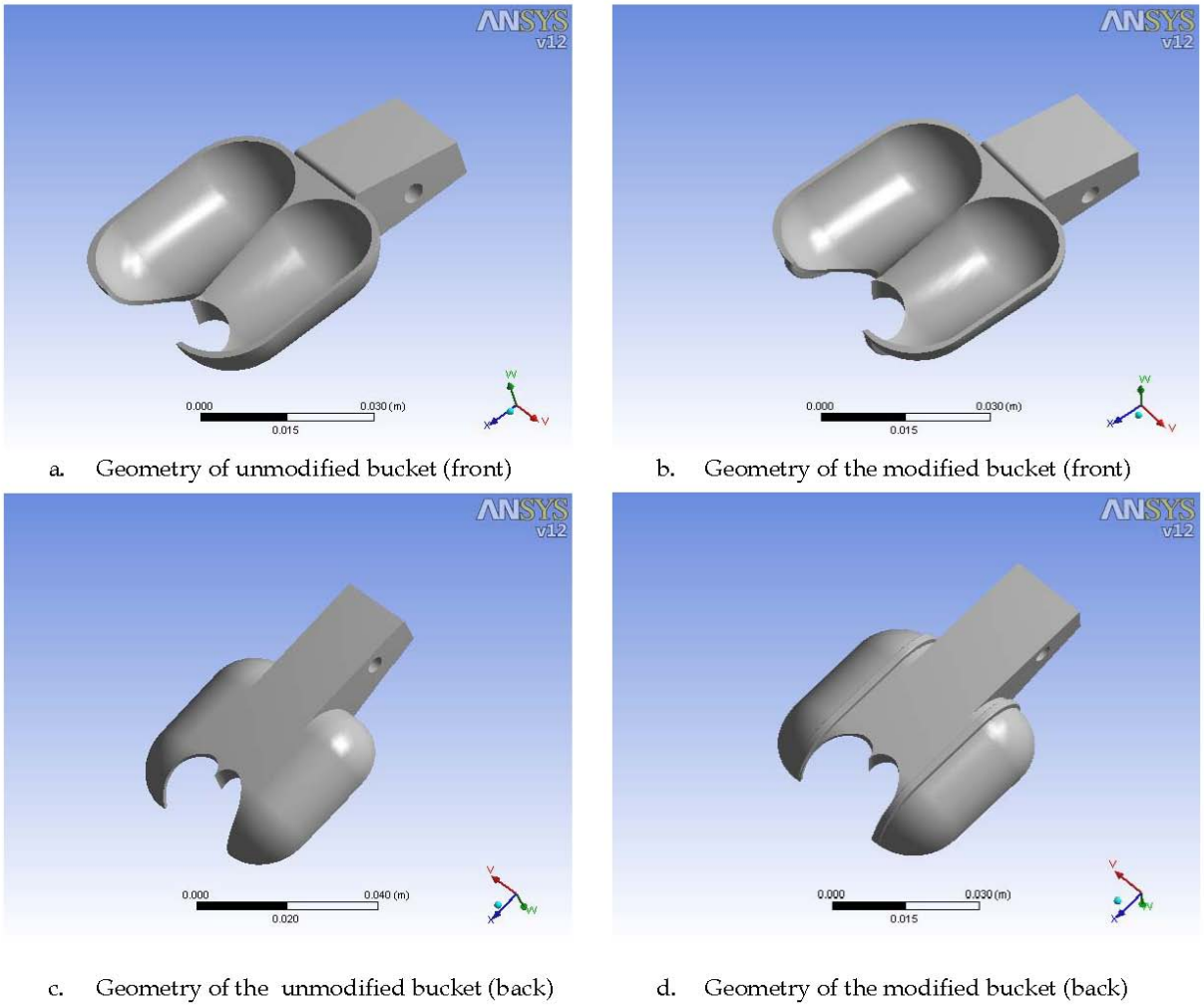

a. Geometry of unmodified bucket (front)

b. Geometry of the modified bucket (front)

c. Geometry of the unmodified bucket (back)

d. Geometry of the modified bucket (back)

Figure 3.4: Geometry of the Pelton bucket

For this research work p-method of ANSYS was used to obtain results for deformation and stresses on the buckets to a specified degree of accuracy using convergence method. To solve for the results, the p-method manipulates the finite element shape functions used to approximate the real solution. The steps followed are shown in Figure 3.5.

The procedure for a p-method static analysis consists of four main steps which

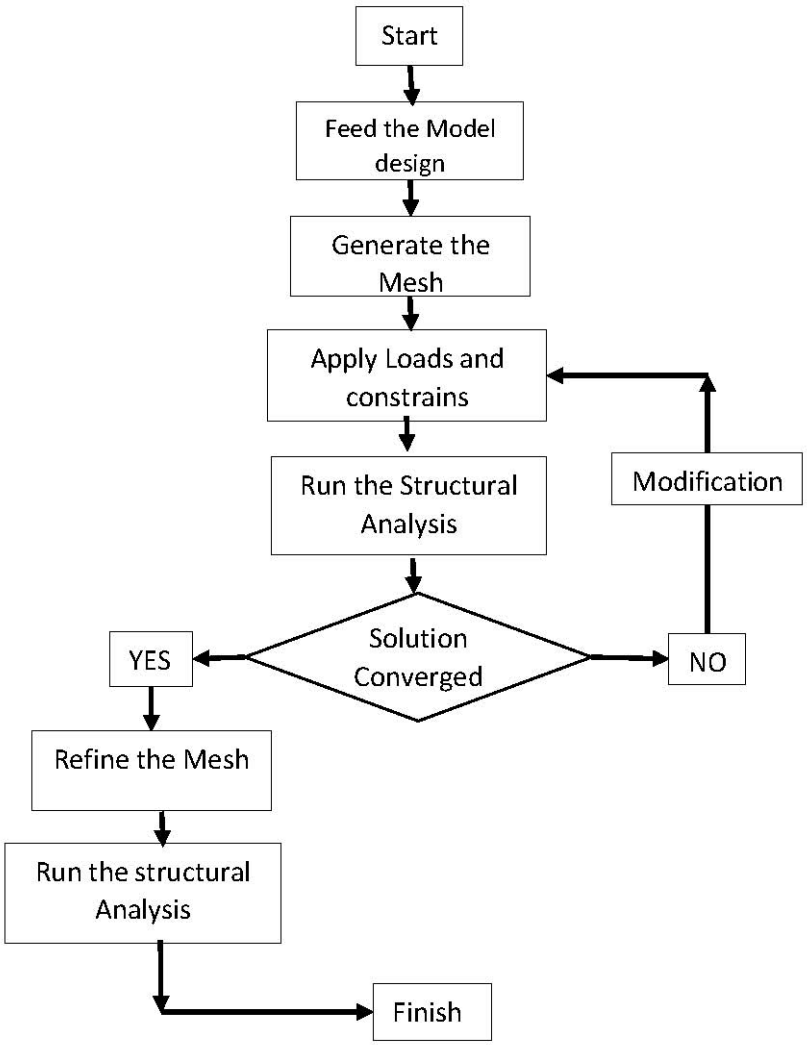

Figure 3.5: Simulation Flow Diagram

include; building the model, applying loads and constrains, obtaining the solutions and finally reviewing the results. Modeling and simulation results are discussed in the chapter that follows.

3.5.1 Pelton Bucket Modeling

The model was created using Inventor CAD techniques and exported to ANSYS software. After generating the solid model, meshing was done with P-elements. 3-D

tetrahedron elements were preferred over the 2-D elements. Two sets of mesh with different degree of fineness were used in this analysis. The first set of models were defined as coarse mesh and in this case fast solution and results were obtained but with significant uncertainty. The meshed models are shown in Figure 3.6.

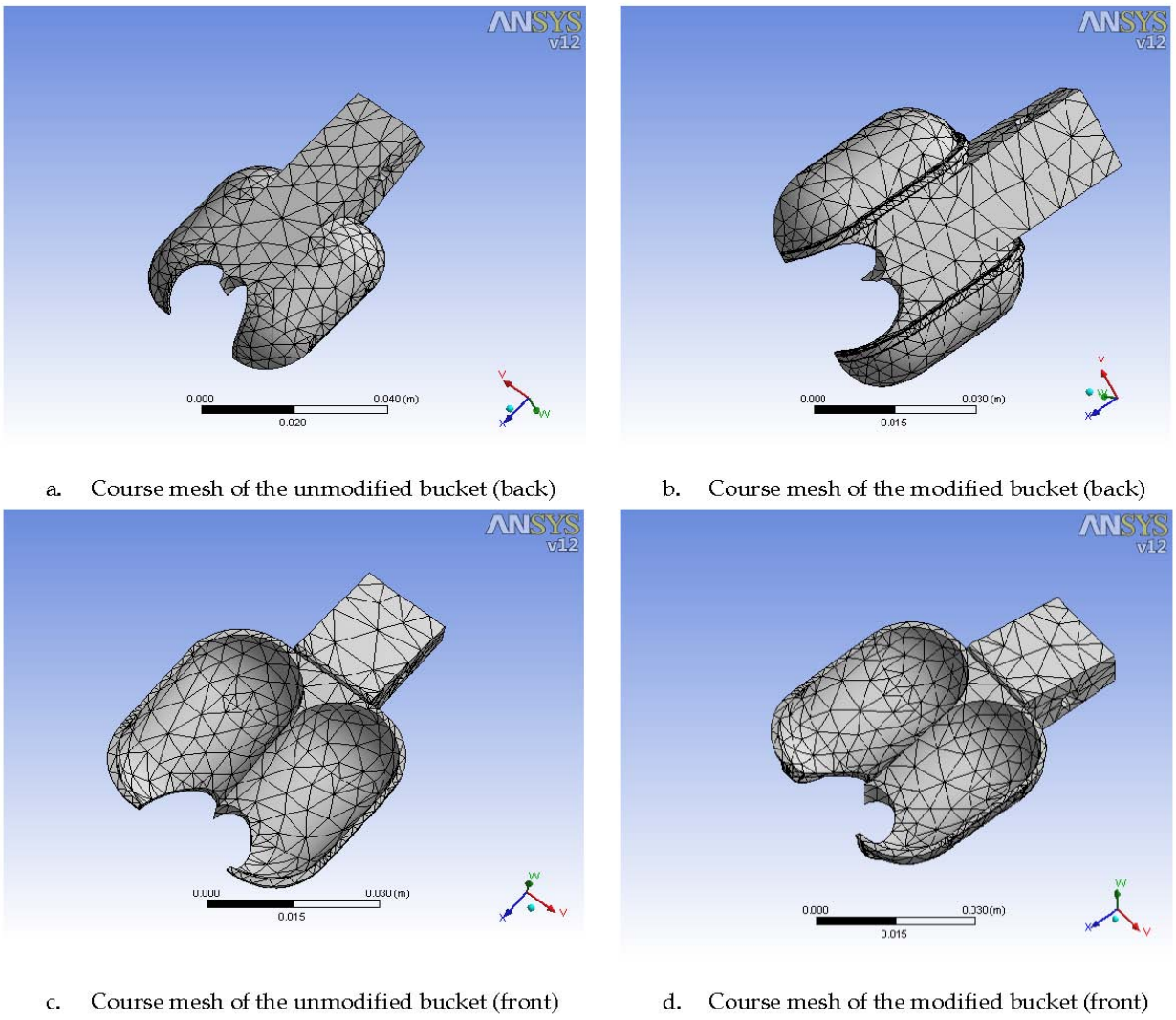

a. Course mesh of the unmodified bucket (back)

b. Course mesh of the modified bucket (back)

c. Course mesh of the unmodified bucket (front)

d. Course mesh of the modified bucket (front)

Figure 3.6: Coarse mesh of the Pelton bucket

To improve on this, a second set of mesh referred to as fine mesh was generated. Longer solution time was used and results had less uncertainty. The refined meshed models are shown in Figure 3.7. From the simulation it was possible to generate the two sets of meshed models automatically by setting the relevance levels to the

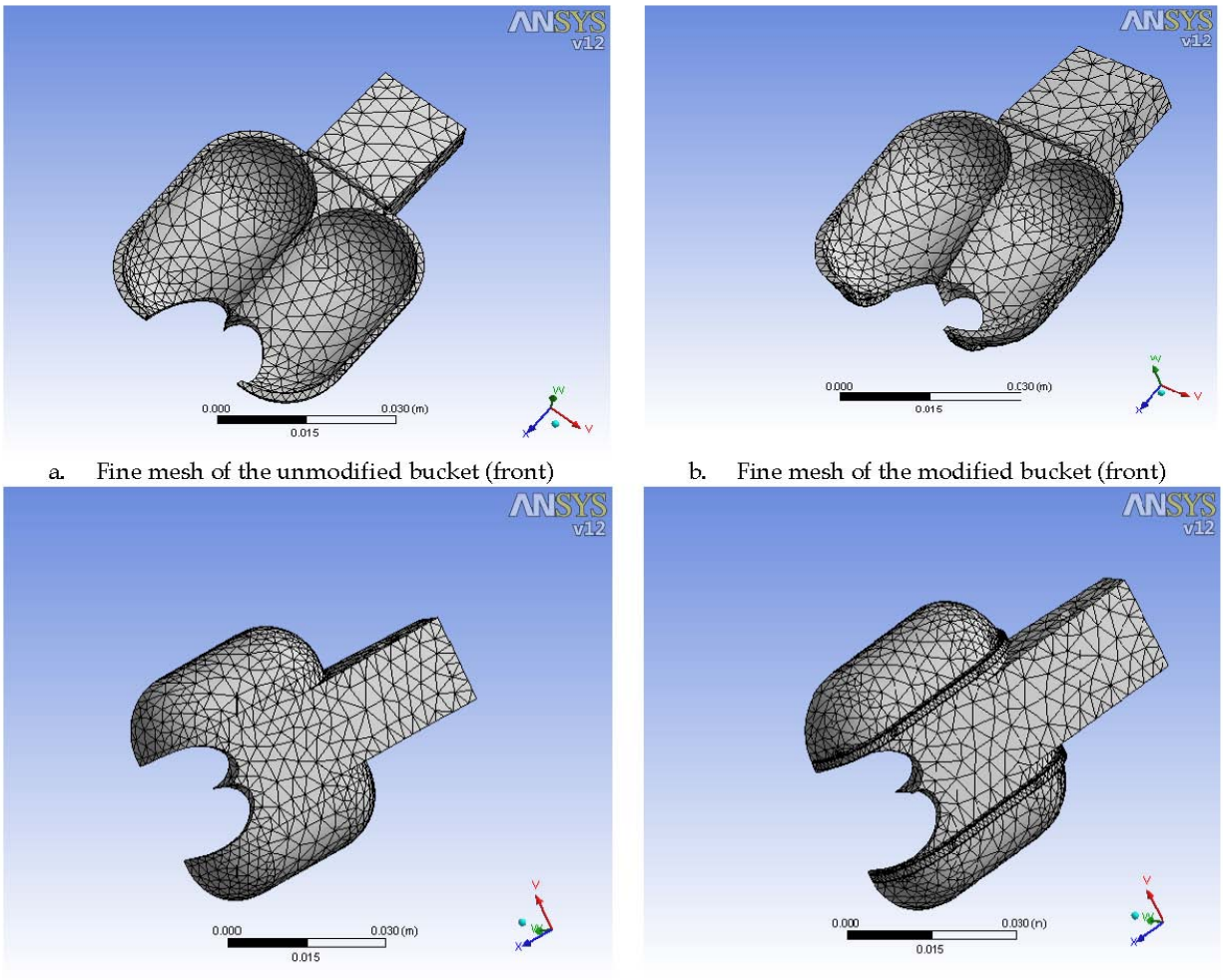

a. Fine mesh of the unmodified bucket (front)

b. Fine mesh of the modified bucket (front)

c. Fine mesh of the unmodified bucket (back)

d. Fine mesh of the modified bucket (back)

Figure 3.7: Refined mesh of the Pelton bucket

extremes. A relevance setting between -100 and +100 controlled the fineness of the mesh used in this analysis. A setting of -100 produced the coarse mesh and setting of +100 generated the fine mesh. Details of the bucket for midway relevance setting '0' are shown in Table 3.1. The ANSYS system manipulated each element's p-level during solution to obtain accurate and efficient results in a process explained below as discretization.

Table 3.1: Buckets statistics for fine mesh

Unmodified Bucket Part Statistics		**Modified Bucket Part Statistics**	
Bounding Box Dimensions	45.05 mm	Bounding Box Dimensions	45.05 mm
	12.55 mm		14.04 mm
	64.2 mm		64.23 mm
Part Mass	2.197e-002 kg	Part Mass	2.267e-002 kg
Part Volume	8106 mm^3	Part Volume	8364 mm^3
Mesh Relevance Setting	0	Mesh Relevance Setting	0
Nodes	4066	Nodes	6656
Elements	2133	Elements	3250

3.5.2 Model Discretization

The mesh was refined on the buckets curved surface where greater variation in results parameters being computed were expected. Specifying meshing controls to finer value helped obtain the desired accuracy near the curved areas of interest. The elements in these areas are smaller relative to the other areas of the model and a transition region occurs from the large to the smaller elements.

3.5.3 Loads and Constrains

The conditions set on the bucket model defined the material properties and the boundary conditions were set as explained in the steps below.

3.5.4 Material Properties and Constants

Material properties for isotropic p-elements with constant temperature were used. In order to carry out structural analysis with inertia loads such as gravity the density of the material denoted as (DENS) was specified which was required for mass calculations. Young's Modulus (EX) was defined. The following material behavior were applied to this analysis. Stress was assumed to be linear and directly proportional to strain. The composition structure of the material was assumed to be homogenous and did not change throughout the volume of the part and was Isotropic such that the material properties are identical in all directions. A356 aluminum

casting alloy has very good casting and machining characteristics and is used for turbines, pump housings, impellers, high velocity blowers and structural castings where high strength is required. It can also be used as a substitute for aluminum alloy Al6061, Casting the bucket using investment casting that heat treats Al A356 an equivalent of Al6061 was used for simulation. According to American Foundry Society A356 aluminum casting alloy can also be used as a substitute for aluminum alloy 6061 (Yury S. et al., 2013).

3.5.4.1 Boundary Conditions

Figure 3.8 depicts the computational domain and the boundary conditions applied. Two forces on each half of the bucket of 1236.8 N were applied and a fixed support on the root of the bucket. The incoming jet was assumed to be ideal, with a constant velocity profile determined numerically from the specific energy and discharge conditions, and the flow relative to the splitter to be symmetrical.

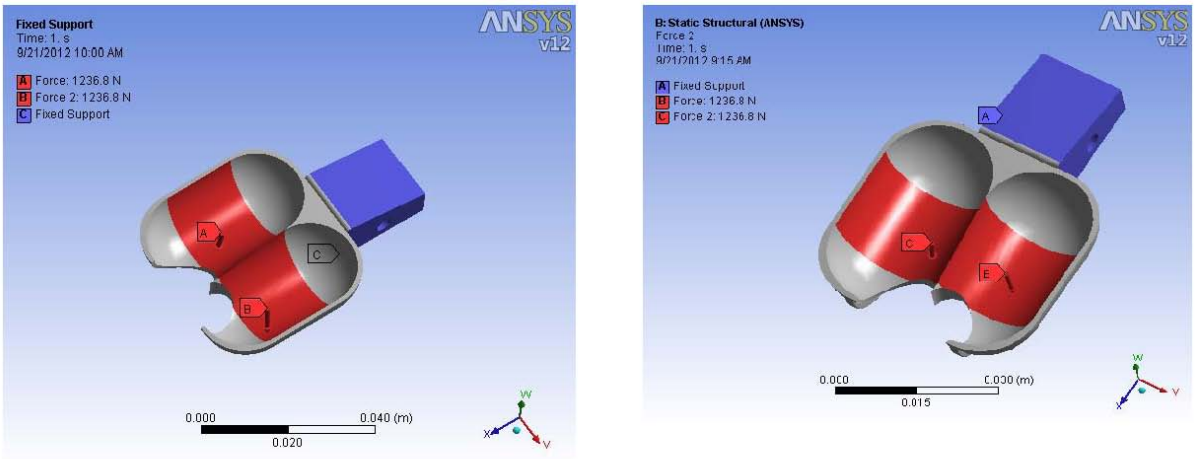

a. Loading on the unmodified bucket

b. Loading on the modified bucket

Figure 3.8: Loading on the Pelton bucket

3.6 Experimental Methodology

In the following sections the experimental procedures of this research are explained in detail. To validate the numerical results, bending experiments were car-

ried out on bending testing machine as explained in this chapter. To assess the Pelton turbine operations, failure and efficiency, a field survey was carried out on Kathamba community hydro power plant in Kirinyaga district. The plant utilizes a Pelton turbine which has an electrical output of 1.1 kW. This supplies power to 65 households using a single-phase distribution system. The main challenge of the system was that the power output was not enough to serve all the connected customers. When the demand for power was high, the turbine was run above the full capacity. This caused frequent failure on the bearings. The mode of failure was analyzed and discussed in the subsequent chapter.

3.6.1 Pelton Turbine Design

The Pelton turbine was designed on the basis of the input data which was the available discharge, the head and the rotational speed. The first step of the design process involved calculating the specific speed coefficient which was the ratio between the velocity of turbine and that of the water jet. Subsequently the water jet speed was regulated to reach the desired specific speed coefficient. Figure 3.9 illustrates the schematic views of a pelton turbine and the bucket (Logan 2003).

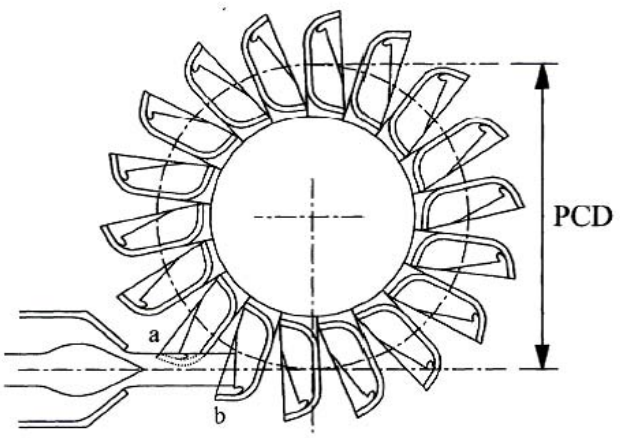

Figure 3.9: Features of Pelton turbine (a) nozzle and water jet (b) Pelton runner (Logan 2003)

To maximize the turbine driving force developed from the water jet, the bucket

was set perpendicular to the jet. There was however, the practical issue of clearing the water for the next bucket and therefore the bucket was set at an angle of 15^o which provides enough clearance while keeping the force high.

The buckets were made in a hemispherical shape in order to ensure the jet was deflected through 180^o. The relative velocity of the jet leaving the bucket was opposite in direction to the relative velocity of the jet entering. This was difficult to achieve practically because the jet leaving the bucket then strikes the back of the succeeding bucket and hence overall efficiency was decreased. Therefore in practice the angular deflection of the jet in the bucket was limited to about 165^o, and the bucket was slightly smaller than a hemisphere in size. The bucket was assumed to be permanently fed by the full jet impinging on the splitter with an angle of attack equal to 90^o. Convectional design guide lines have been developed as illustrated in Figure 3.10. The figure shows the relationship of the bucket dimensions as a percentage of the Pitch Circle Diameter (PCD) of the turbine (Chepuis L. et al., 1998).

3.6.2 Test Bucket Production

After determining the Pelton turbine size, the next step was to develop a CAD drawing of the bucket using the empirical relations as discussed in the sections that follow. CAD drawing of the Pelton bucket was made using Autodesk software. This helped in production of the bucket with more precise dimensions and material consistency. Computer-aided manufacturing (CAM) was then implemented by running the computer software (the G-codes) to control related machinery in the manufacturing of master pattern. Its primary purpose was to create a faster production process, components and tooling with more precise dimensions. Material consistency, which in this case, used only the required amount of raw material (thus minimizing waste), while simultaneously reducing energy consumption. Computer Numerical Controlled (CNC) programming and simulation was developed using OneCNC soft-

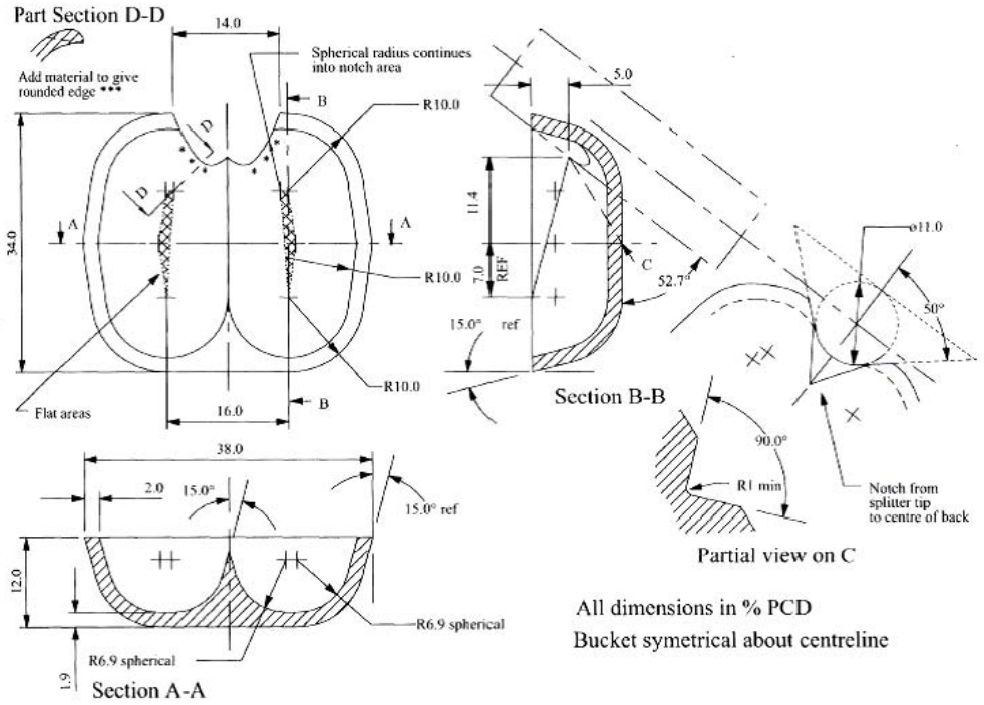

Figure 3.10: Conventional Pelton bucket dimensions

ware at Ashikaga Institute of Technology (Japan). An electronic database in form of G-codes used for machining the master pattern was created. This was then exported to a CNC machine. Production of the master pattern from a high density plastic was done and the pattern used to carry out casting. The test bucket drawn using Autodesk software is shown in Figure 3.11. Simulation of the G-codes is shown in Figure 3.12. CNC machining done to produce the master pattern from a high density plastic is illustrated in Figure 3.13.

The final master bucket was obtained as shown in Figure 3.14. CAD drawing based on the empirical dimensions of a 1 kW Pelton bucket was made using Autodesk software.

3.6.3 Casting Process

The current concern amongst manufacturers of turbines is keeping maintenance costs and repairs to minimum with higher component reliability. Casting as one of

Figure 3.11: Autodesk Pelton bucket drawing

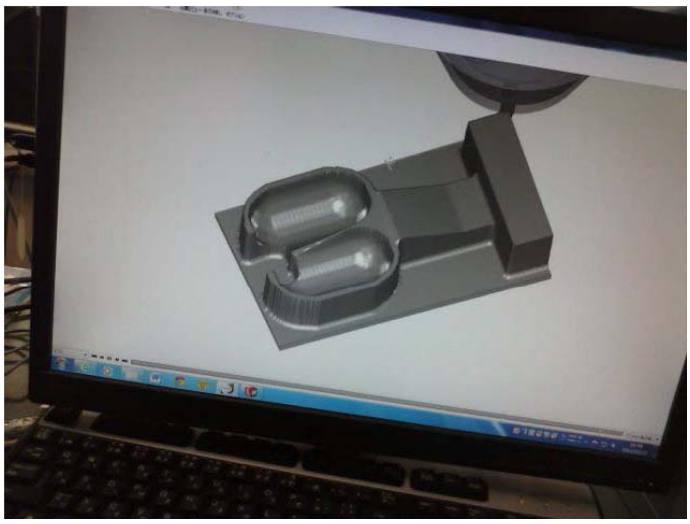

Figure 3.12: G-code simulation of the bucket

the viable fabrication techniques due to the complex shape of the bucket and the ease of reproducing the buckets was adapted (Gilbert G. et al., 2003). The test buckets were produced using casting technique, thus on the dimensions contraction and shrinkage allowances were taken into consideration. Aluminium A356 alloy produced from recycled automotive rims of mechanical property shown in Table 3.2 was used to cast the test buckets. Two methods were used to produce the test buckets, that is investment casting and sand casting.

Figure 3.13: Master bucket production on a CNC machine

Figure 3.14: Pictorial views of the master bucket

Table 3.2: Mechanical property of Aluminium A356 alloy

A356.0 –T6	**Values**
Tensile Strength, Ultimate, Mpa	282.68
Tensile Strength, Yield, Mpa	206.84
Elongation %; break	82.73

Figure 3.15 shows the process involved in investment casting for production of the Pelton bucket. From the machined bucket pattern, rubber mold was made from which wax patterns were produced. What followed was a process that involved making a ceramic mould, known as the investment. The wax pattern was placed in a flask and then liquid investment material (plaster) poured into the flask. The flask was then vibrated by tapping the sides to allow entrapped air to escape and help the investment material fill in all of the details. The investment was then allowed to completely dry. After that, it was then turned upside-down and placed in a furnace to melt out the wax. In this case, dewaxing was also used as preheat and burnout process. Any wax that runs out of the mold is usually recovered and reused. The mould is preheated to allow the metal to stay liquid longer to fill any details. This also increases dimensional accuracy, because the mold and casting cool together. The metal was gravity poured and allowed to solidify. Finally the ceramic shell was broken off to release the casting. The sprue were cut off and recycled for the next casting. Another technique of sand casting was utilized to produce the final buckets used to carry out experiments. This is a practice that uses a model of the object to be produced. A hollow mold was made using moist sand and clay mix (molding sand). Molten metal was then poured into the mold and allowed to cool and solidify. This research utilized aluminium A356 which is a recycled alloy with chemical composition as shown in Table 3.3. Once the parts were obtained the

Table 3.3: Chemical composition of Aluminium A356 alloy

Component	**Si**	**Cu**	**Mg**	**Ti**	**Fe**	**Mn**	**Zn**	**Al**
Wt %	6.5-7.5	Max 0.2	0.25-0.45	Max 0.2	Max 0.2	Max 0.1	Max 0.1	93

first step was to inspect them. Components with large defects or holes and castings having excessive shrinkage were rejected. The root is important because this is machined to provide reference surfaces and ensure that all the buckets are correctly aligned when assembled on the turbine hub. The casted buckets were carefully fettled to remove excess metal which had resulted from the casting process. For

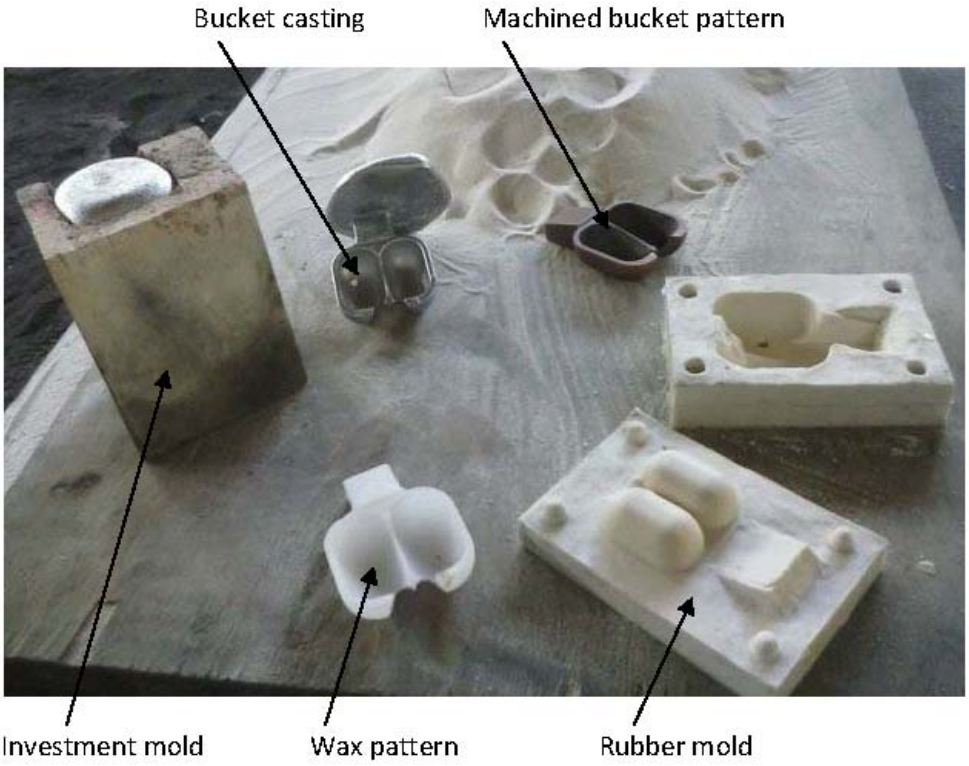

Figure 3.15: Test Buckets production from Investment Process

the buckets, careful finish on the back of notch was done by filing. The front edge of the notch should be sharp. Filing was done to the required dimension ensuring particular care not to remove too much material. The inside surfaces of the buckets were polished with emery cloth. Surface roughness of the individual buckets can cause a significant reduction in overall performance of the runner. The buckets roots were filed to ensure an equal distance between the side of the root and the splitter ridge on each bucket. This allowed the bucket center to align when bolted on to the turbine hub.

Additional work in this research was to produce the modified buckets from existing ones. Modification was done to produce the casting patterns of the modified bucket using body filler. The dimensions of the bucket which was used in stress analysis and experiments are shown in Figure 3.16.

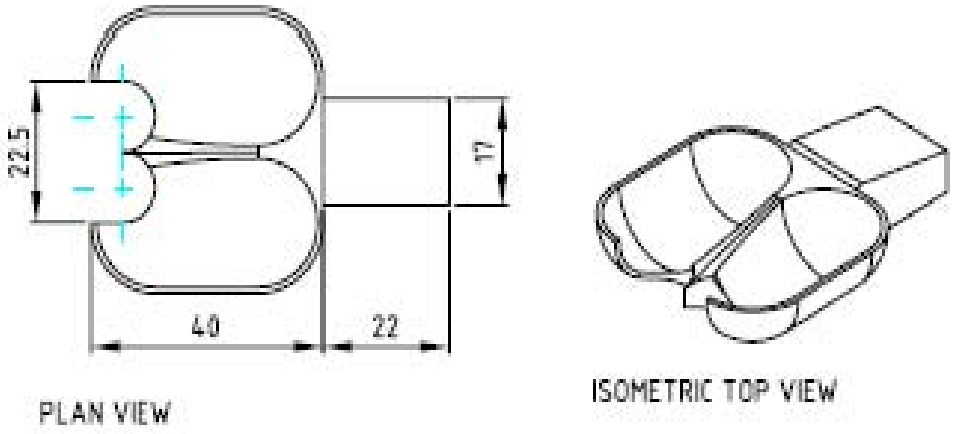

Figure 3.16: Bucket dimensions (mm)

3.7 Model Validation

The classical beam theory method to determine the stress in the Pelton bucket was used treating the bucket as a point-loaded beam clamped at its root. This method delivered conservative results and lead to very reliable mechanical designs for the normal range of Pelton turbines (Alexandre P. et al., 2005). Three tests were carried out on a bending testing machine shown in Figure 3.17. The test carried out included; bucket bending deflection, bucket bending strength and bucket pull-out force.

The experimental setup is as shown in Figure 3.18. Selected range of results for deflection against applied load were used to counter-check the simulation results. A suitable load was used that would not deform the bucket out of the elastic region, but would give a deflection that was large enough to be measured reliably. Equivalent force to the jet force at different heads and for different nozzle diameters as calculated in the in the previous chapter were applied on the clamped bucket. Plastic deformation of the bucket was monitored and recorded until the bucket broke under bending force.

After the numerical calculation and the experimental validation results were

Figure 3.17: Bending testing machine used for experiments

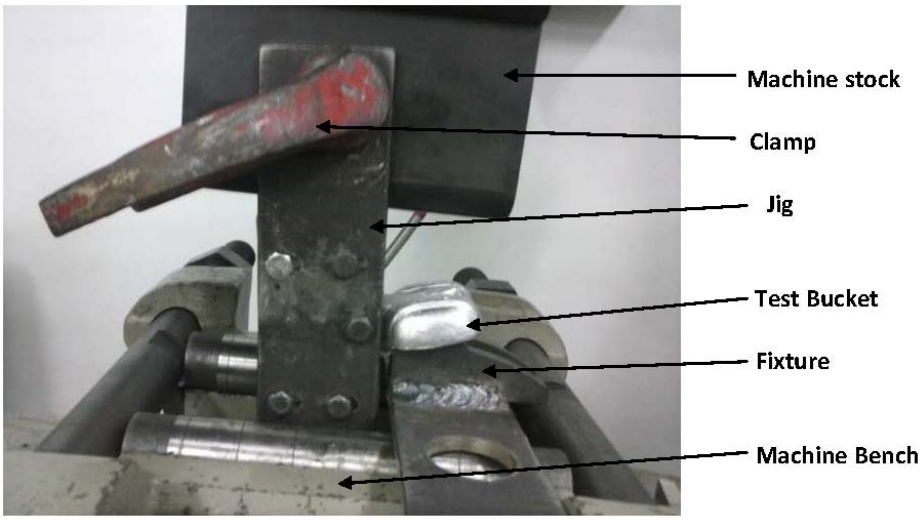

Figure 3.18: Bucket bending test

obtained and are discussed in the following chapter.

CHAPTER FOUR

RESULTS AND DISCUSSION

4.1 Background

Demand for more power from small turbines leads to overloading the turbine by operating them at higher heads and flow rate conditions than the design values. This subjects the runner to stresses caused by centrifugal forces and cyclic loads due to high rotational speeds and high pressure on the turbine runner. The runner is vulnerable to failure due to excessive loading and in this Chapter results for the work carried out as explained in the methodology chapter are discussed in details. This includes modeling and simulation results and experimental results. Optimum operating conditions for 152 mm PCD Pelton turbine that would not fail under cyclic loading were obtained. ANSYS structural was used to simulate the mechanical behavior of the models under structural loading conditions and to generate simulation results presented in this chapter. In order to validate the numerical results of the bucket models physical testing on the two bucket models were carried out. Evaluation of the bucket designs was done by comparing the simulation results with experimental tests results.

4.2 Numerical Modeling

Two parameters were examined to obtain variations in the initial driving force of a turbine. These were the head and the nozzle diameter. The head was the pressure created by the difference in elevation between the intake of the pipeline and the water turbine. The head was measured as vertical distance (meters) or as pressure (newtons per square meter). A nozzle is a device designed to control the direction or characteristics of a fluid flow (especially to increase velocity) as it exits an enclosed chamber or pipe. A single nozzle are used to control the rate of flow, speed, direction, mass, shape and the pressure of the stream water that emerges from them. The water jet force that drives the turbine was computed for head

variations between 15 m and 60 m and obtained to be between 275.3 N and 1105.2 N as shown in Table 4.1.

Table 4.1: Data for Head Variation between 15 m and 60 m

Flow rate Q (m^3/s)	Static head (m)	Nozzle diameter (m)	Friction coef.	Reynolds no.	Nozzle velocity (m/s)	Jet power (W)	Turbine power (W)	Turbine speed (rpm)	Bucket velocity (m/s)	Mass flow rate (m^3/s)	Force (N)
0.0183	15	0.01905	0.018	152,934	15.93	2355	1,060	1,006	8.0278	17.8037	275.316
0.0227 2	22.5	0.01905	0.018	189,850	19.51	4504	2,027	1,248	9.9656	21.8042	407.227
0.0261 9	30	0.01905	0.018	218,854	22.56	6901	3,105	1,439	11.4881	25.2114	546.154
0.0292 8	37.5	0.01905	0.017	244,695	25.24	9645	4,340	1,609	12.8445	28.2099	684.345
0.0321 8	45	0.01905	0.017	268,954	27.65	12807	5,763	1,769	14.1179	30.9083	818.818
0.0369 1	60	0.01905	0.017	308,506	31.99	19329	8,698	2,029	16.1941	35.7527	1105.17

The jet force computed for nozzle diameter variations between 0.0254 m and 0.0127 m was obtained to be between 309.2 N and 1236.8 N as shown in Table 4.2. Calculations were based on the formulas presented in the earlier chapter as numerical calculation. The water jet forces limits were set for calculated power output between 1 kW and 10 kW for 152 mm PCD Pelton turbine.

Table 4.2: Data for Nozzle Diameter between 0.0254 m and 0.0127 m

Nozzle diameter (m)	Friction coef.	Reynolds no.	Nozzle velocity (m/s)	Water jet power (W)	Power at turbine wheel (W)	Bucket velocity (m/s)	Mass flow rate (l/s)	Force (N)
0.0127	0.018	218,854	50.86	34,934	15,720	25.8483	25.265	1236.8
0.01397	0.018	218,854	42.03	23,860	10,737	21.3622	25.265	1022.1
0.01524	0.018	218,854	35.32	16,847	7,581	17.9502	25.265	858.89
0.01651	0.018	218,854	30.09	12,231	5,504	15.2948	25.265	731.83
0.01778	0.018	218,854	25.95	9,094	4,092	13.187	25.265	631.02
0.01905	0.018	218,854	22.60	6,901	3,105	11.488	25.265	549.69
0.02032	0.018	218,854	19.87	5,330	2,399	10.096	25.265	483.12
0.02159	0.018	218,854	17.60	4,183	1,882	8.9440	25.265	427.95
0.02286	0.018	218,854	15.70	3,328	1,498	7.9778	25.265	381.72
0.02413	0.018	218,854	14.09	2,681	1,206	7.1601	25.265	342.60
0.0254	0.018	218,854	12.71	2,183	983	6.4620	25.265	309.20

Figures 4.1 shows variation of head between 15 meters and 55 meters with corresponding power output between 1 kW and 8.5 kW. Higher heads have higher hydraulic potential power thus higher jet forces on the bucket. It was observed that hydraulic potential power was directly proportional to the head, H.

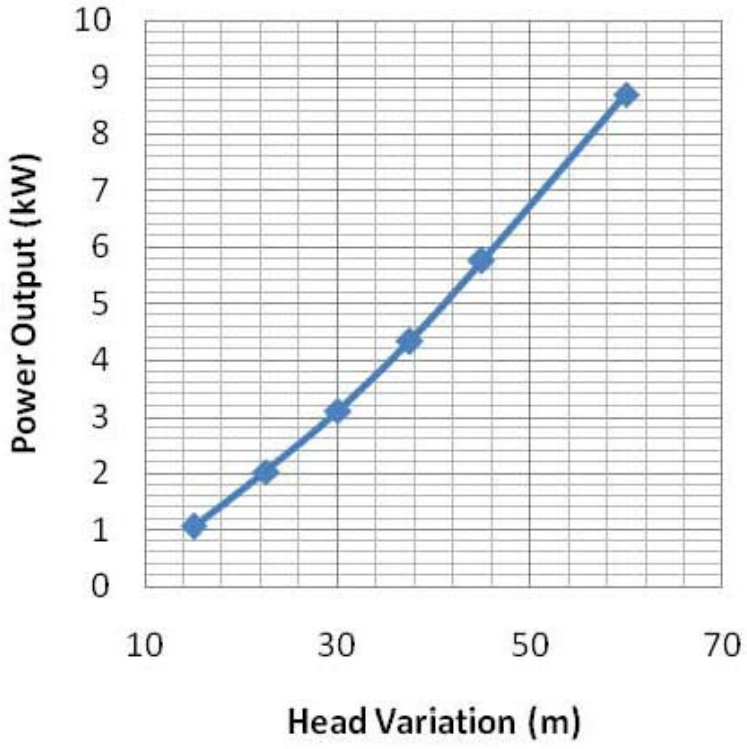

Figure 4.1: Head variation vs power output

Figure 4.2 shows variation of head between 15 meters and 55 meters with corresponding jet force. Higher heads resulted to higher hydraulic potential power thus higher jet forces on the buckets. It was observed that jet force was directly proportional to head, H.

Figures 4.3 show variation of nozzle diameter between 0.0125 m and 0.0275 m with corresponding power output and jet force. By reducing the nozzle diameter for a constant flow rate the velocity of fluid was increased but the pressure energy reduced. The goal was to increase the kinetic energy of the flowing water at the expense of its pressure and internal energy of a given head. This brings an increase in the jet force and thus the power output of the turbine.

The velocity of the jet was inversely proportional to the diameter of the nozzle and this was depicted in Figure 4.4. The figure shows how forces developed by the water jet as a result of nozzle diameter reduction are related.

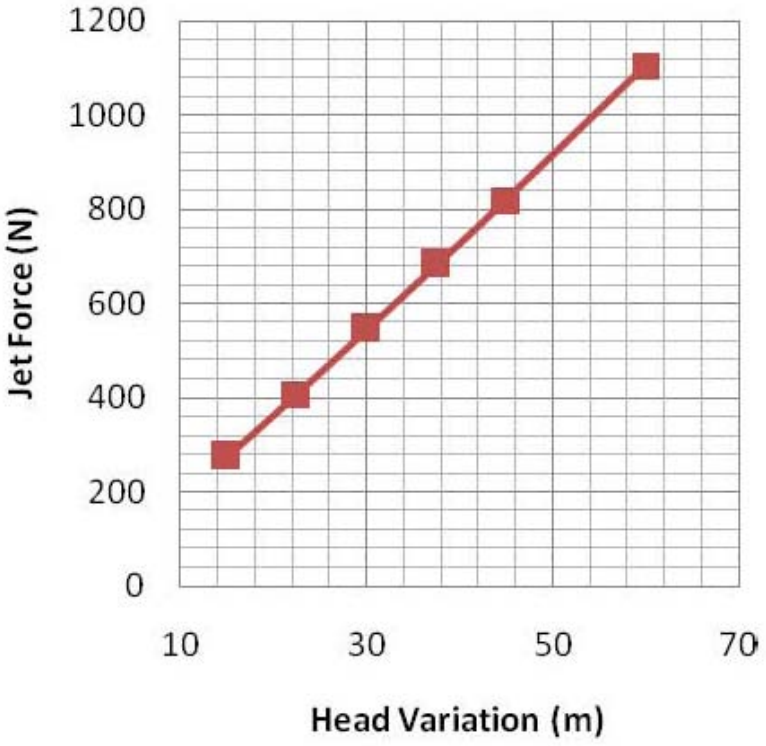

Figure 4.2: Head variation vs equivalent jet force

From the graph, a reduction on the nozzle diameter increases the jet velocity and thus the kinetic power of the water jet. It was observed that more power is delivered from the turbine as a result of nozzle diameter reduction. The power increased proportionately with reduction in nozzle diameter between 0.0254 m and 0.0175 m then further reduction on the nozzle diameter caused a rapid increase in the kinetic force on the bucket accelerated fatigue failure in the turbine buckets.

4.2.1 Modeling Results

The accuracy of the performance of the simulation was determined from the convergence criteria. This was based on concurrent iteration/cycle, force convergence, displacement convergence and time steps. The solutions converged after 13 iterations as shown in Convergence plot in Figure 4.5.

The frequency at which data was generated was specified as a time step fre-

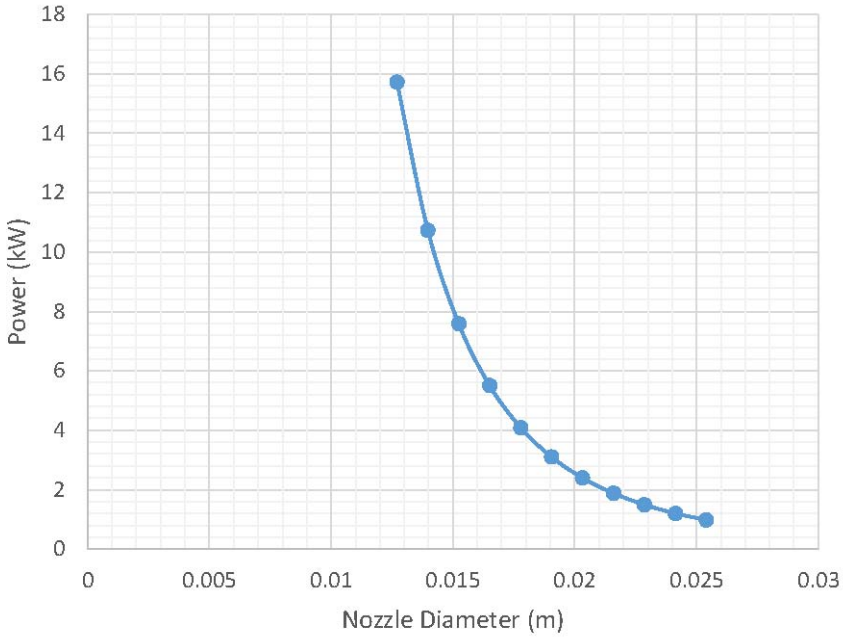

Figure 4.3: Nozzle variation vs power output

quency. Information was displayed for every 10 seconds. Review on the results, was done through tracking, monitoring and diagnosing problems that arose during solving.

4.3 Simulation Stress Analysis Results

Stress analysis of unmodified and modified bucket were done with the help of ANSYS Structural software. Effect of modification on the bucket profile on stress developed was depicted. The different jet loads on the bucket deduced from the numerical calculations were used as the input conditions for the structural analysis in ANSYS simulation.

The simulation results of principal stresses developed on the two bucket models are shown in Figure 4.6. From the graph the equation showing the relationship between stress and jet force for the modified buckets was obtained to be;

$$\sigma_p = 0.20F \tag{4.1}$$

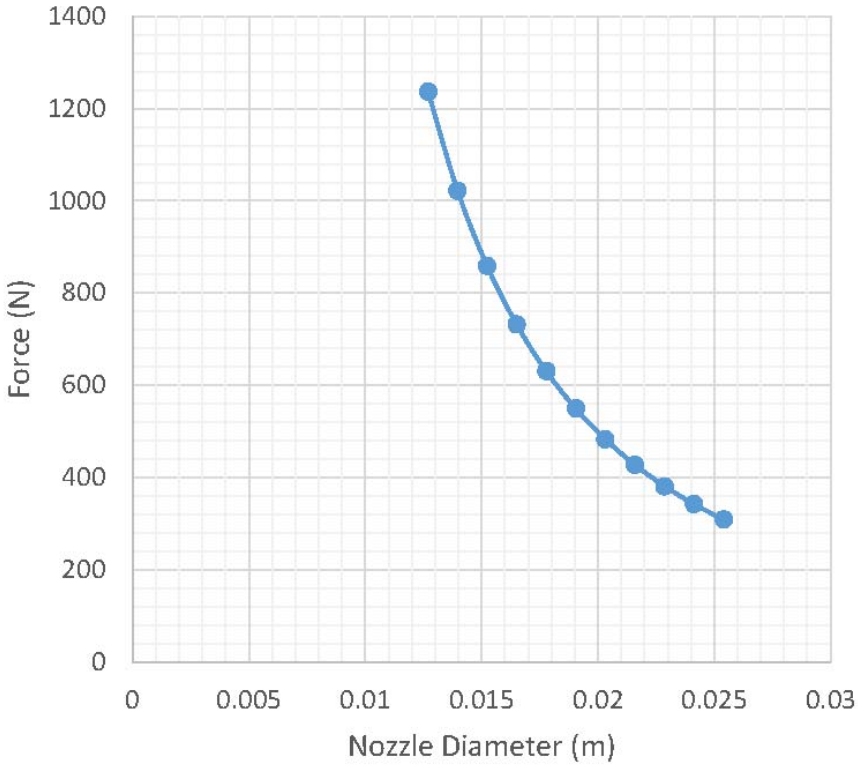

Figure 4.4: Nozzle variation vs equivalent jet force

where σ_p is the maximum principal stress and F is the jet force. And that of the unmodified bucket was obtained to be;

$$\sigma_p = 0.23F \tag{4.2}$$

This shows that stress is directly related to the jet force with a linear average proportionality constant of an avarage of 0.21. By introducing the back ridge, the modified bucket was able to handle more stress than the unmodified. Modified buckets were made by introducing a $2mm$ ridge on each side of the bucket back section.

Patterns of the stress distribution on the buckets are shown in Figure 4.7. The value of the stresses are compared and according to the Von-Mises stress criteria, using applied force of $500N$, the maximum stress for unmodified bucket was found

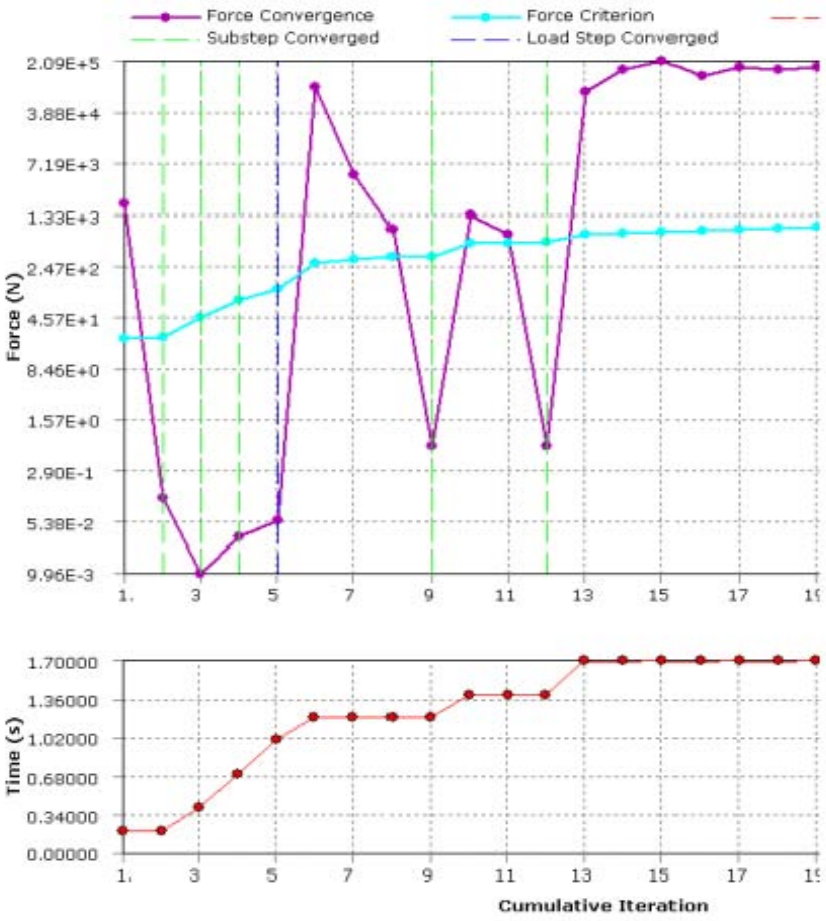

Figure 4.5: Sample of a convergence plot

to be $0.828X10^8Pa$ and that of the modified bucket was $0.795X10^8Pa$.

The graphs depict that the maximum principal stresses developed in the modified bucket are less than those on the unmodified bucket. Stress reduction was calculated to be 14.27%. Modification by introducing the two ridges at the back of the bucket helped in redistributing the stresses on the buckets. For comparison purpose two different models of the buckets were used namely the modified and unmodified buckets and harmonized results were observed. Higher stress values were noted along the Center line of the curved parts of the buckets and highest at the point where it joins the root. This is due to the fact that, as the water changes direction on hitting the buckets most of the energy is absorbed at these points thus

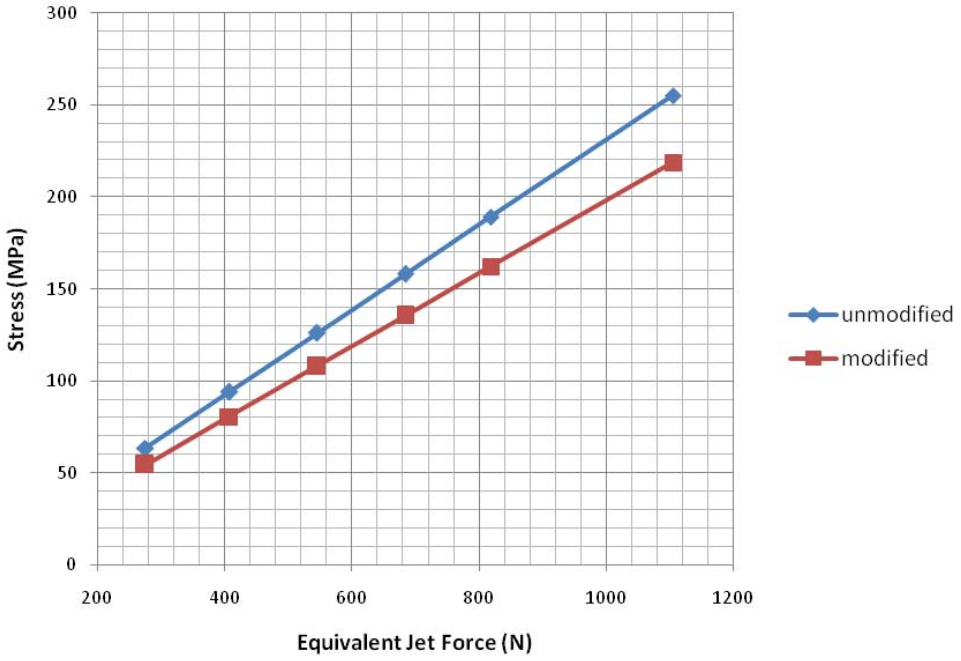

Figure 4.6: Stress due to jet force variation

more stress is developed here. The ridge helps in absorbing and evenly distributing this stresses thus the lower values observed in the modified buckets as indicated in Figures 4.7 b and d. The relationship between stress and head variation within the range of 15 m and 60 m was calculated and plotted as shown in Figure 4.8.

From the graph the equation showing the relationship between stress and head variation for the modified buckets was obtained to be;

$$\sigma_p = 3.652H - 1.245 \tag{4.3}$$

where σ_p is the maximum principal stress and H is the head. The equation for the unmodified buckets was obtained to be;

$$\sigma_p = 4.261H - 1.466 \tag{4.4}$$

The two equations show that the stress increases linearly with increase with head.

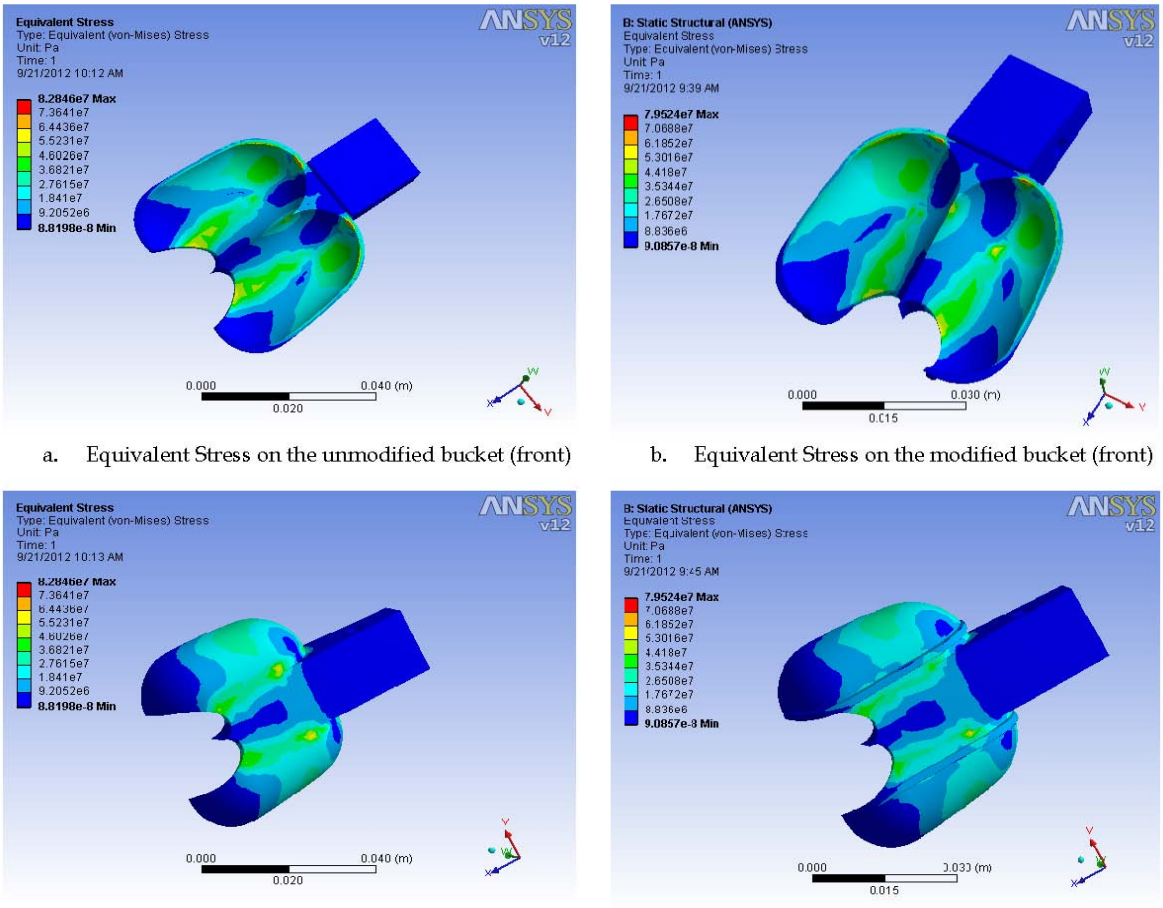

a. Equivalent Stress on the unmodified bucket (front)

b. Equivalent Stress on the modified bucket (front)

c. Equivalent Stress on the unmodified bucket (back)

d. Equivalent Stress on the modified bucket (back)

Figure 4.7: Equivalent stress on the buckets

Based on the yield strength of the aluminium alloy A356 which is around 206.84 MPa that was used, limits were reached at an average head of 52.93 m with an equivalent power output of 6.8 kW.

Also plotted was the relationship between stress and variation in nozzle diameter in the range of 0.0127 m and 0.0254 m as show in Figure 4.9. The Figure shows how stress is related to variation in nozzle diameter. From the graph the equation showing the relationship between stress and variation in nozzle diameter for the

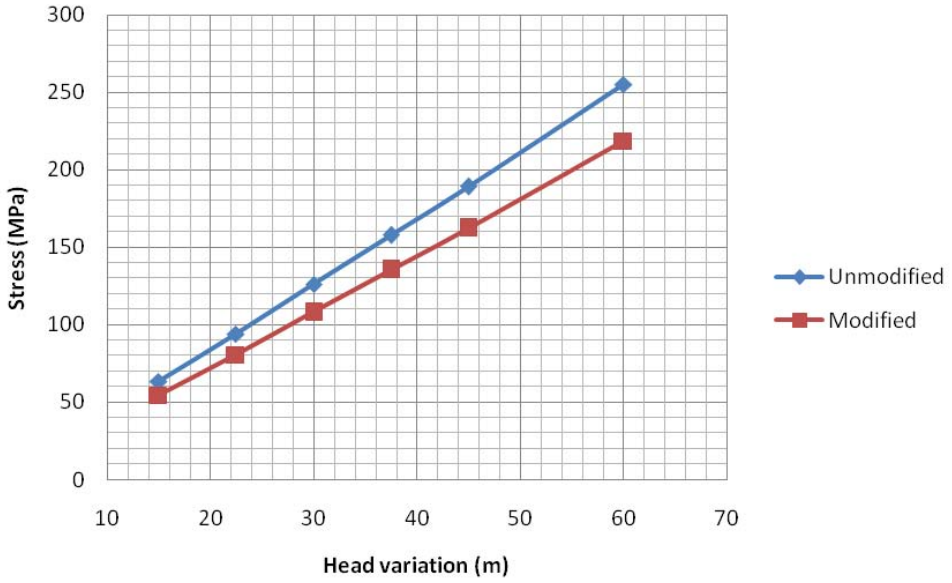

Figure 4.8: Stress due to head variation

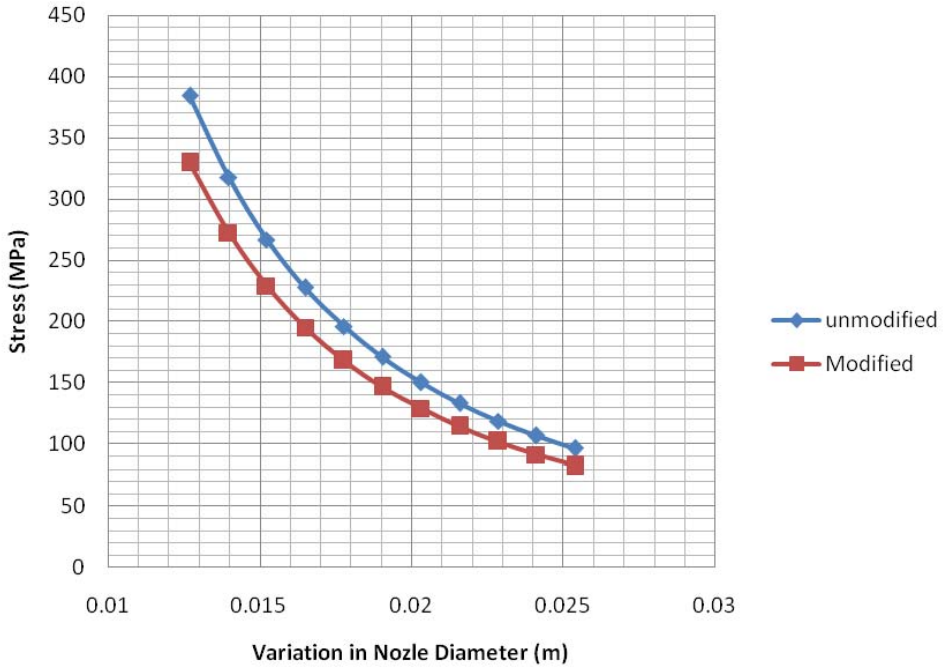

Figure 4.9: Stress due to nozzle diameter variation

modified buckets was obtained to be;

$$\sigma_p = 0.053 D_{jet}^{-2} \tag{4.5}$$

where σ_p is the maximum principal stress and D_{jet} is the nozzle diameter. The equation for the unmodified buckets was obtained to be;

$$\sigma_p = 0.062 D_{jet}^{-2} \tag{4.6}$$

from the equations stress is inversely proportional to the square of the nozzle diameter with an average constant of 0.058 for the two bucket type. At the yield strength of the material used to fabricate the bucket average nozzle diameter was calculated to be 16.66 mm. As a percentage of the turbine PCD of 152 mm of the Pelton turbine this was 10.93% which was in line with the empirical value that state that the nozzle diameter should be about 11% of the turbine PCD. At this nozzle diameter the equivalent power output was obtained to be 5.359 kW. Figure 4.10 shows the relationship between power output and stress for the modified buckets was obtained to be;

$$\sigma_p = 0.535 P^{0.66} \tag{4.7}$$

where σ_p is the maximum principal stress and P is the power output. The equation of the unmodified buckets was obtained to be;

$$\sigma_p = 0.624 P^{0.66} \tag{4.8}$$

An average power output was obtained in case of the two bucket models to be 5.316 kW with an equivalent principal stress of 165.47 MPa which is 80% of the yield strength of aluminium alloy A356 used to fabricate the buckets. This shows that the turbine can be used to generate 5.3 kW of power without failure under stress loading on the buckets.

Figure 4.11 shows structural deflection results generated by the analysis contoured over the surface of the buckets. The ANSYS software calculated safety factor by using the maximum equivalent stress failure theory for ductile materials. The stress limit was specified by the tensile yield strength of the material.

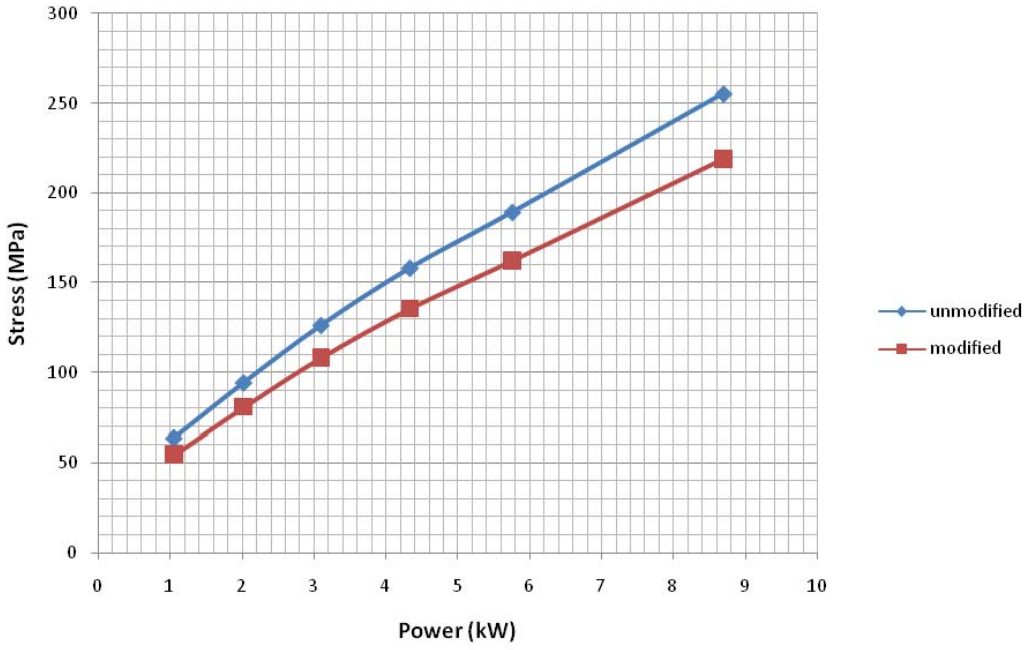

Figure 4.10: Stress against power output

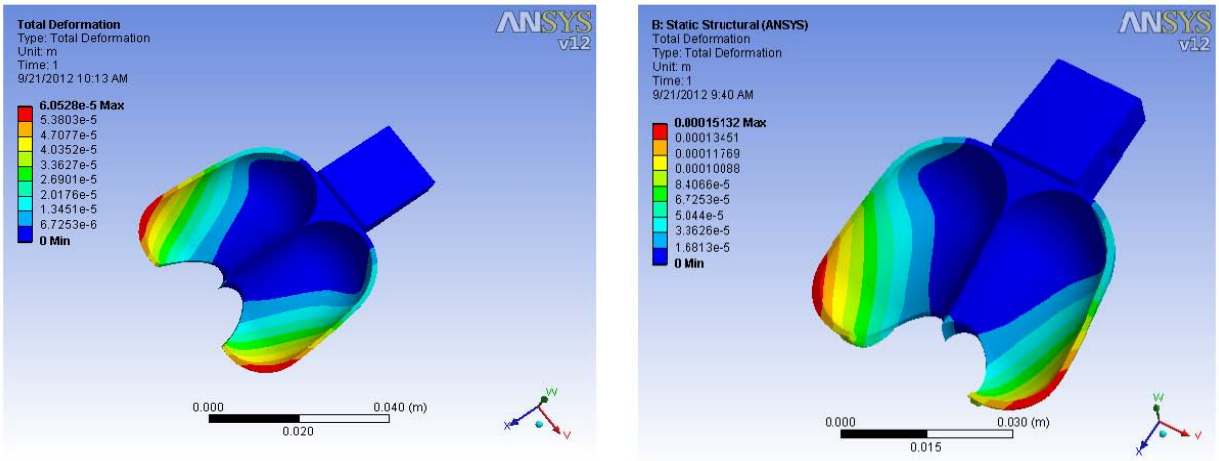

a. Total Deformation on the unmodified bucket

b. Total Deformation on the modified bucket

Figure 4.11: Total deformation on the buckets

4.4 Experimental Tests Results

Bending test was done on the buckets using bending testing machine and loading against deflection graphs obtained. Results within the elastic region for loading force equivalent to jet force of investigation value were deduced. Force against deflec-

tion graph were drawn and compared with the one from simulation using ANSYS. The bucket remained wholly within the elastic region over the test load between 0 and 1236.8 N and linear deformation was observed within the loading range. The comparison graph of load against deflection for the modified and unmodified bucket is show in Figure 4.12.

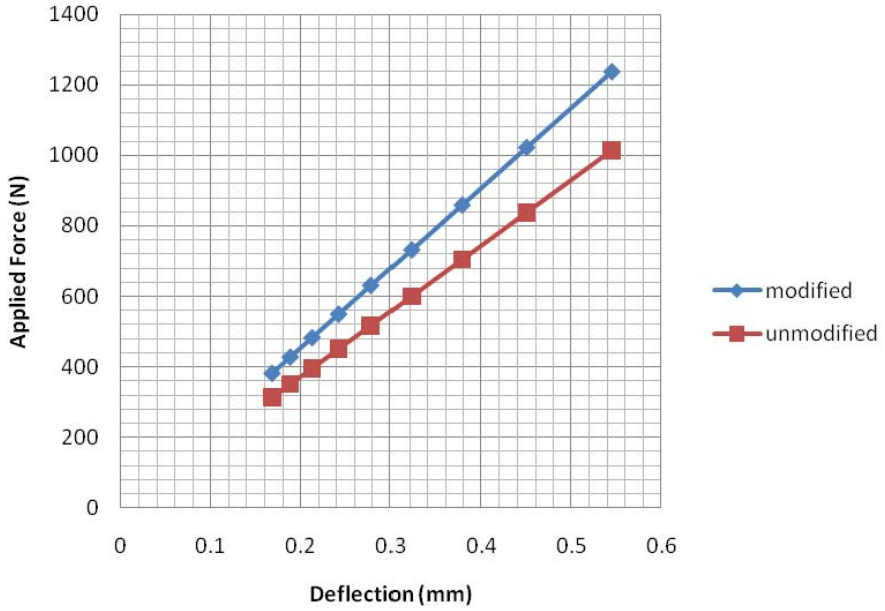

Figure 4.12: Equivalent jet force vs deflection for modified bucket

Using the calculations for equivalent Jet load that indicates the ultimate jet force on the bucket, equivalent amount of force to the clamped bucket was applied until it failed under bending. The modified buckets failed at an average applied force of 8.175 kN with an equivalent stress of 1737.18MPa while the unmodified bucket failed at an average applied force of 6.775 kN with an equivalent stress of 1862.187 MPa. The mode of failure was cracking in the bucket root near the neck radius. The test demonstrated that the bucket has sufficient static strength to withstand any conceivable working jet force for expected power output ranging from 1kW to 10 kW. The power output correspond to stresses ranging between 50 MPa and 210 MPa which are comparable to the yield strength of the aluminium alloy used to produce

the buckets. Treating the bucket as a point-loaded beam clamped at its root the relationship between stress and the applied force was plotted as shown in Figure 4.13. stress is directly related to force within the elastic region of the material.

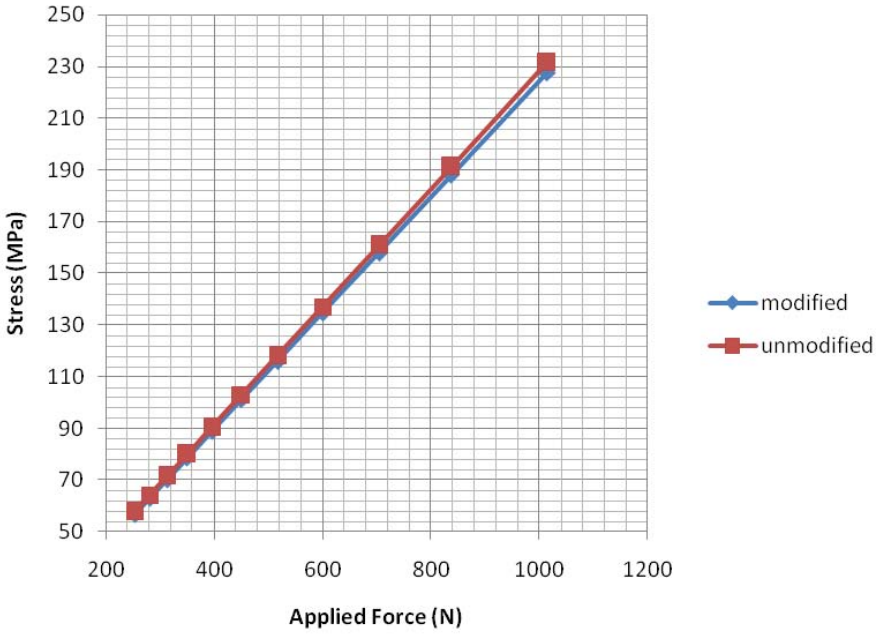

Figure 4.13: Applied equivalent jet force against stresses on the buckets

Having the relationship between force and stress graphs of head variation and nozzle diameter variation within the obtained stress range were plotted and compared with results from simulation. The plots are shown in Figure 4.14 and Figure 4.15 respectfully. As the head increases the resulting stress increases linearly for both in the modified and in the unmodified buckets

The force required to axially displace the clamp was measured and this indicated the level of security of the buckets upon the hub for vertical shaft arrangement. The bucket slipped with an axial load of 12.3 kN.

4.5 Comparison Between Modeling Results and Experimental Results

Comparison of simulation and experiment results for the two main variables i.e the head and the nozzle diameter against stress were done and various graphs

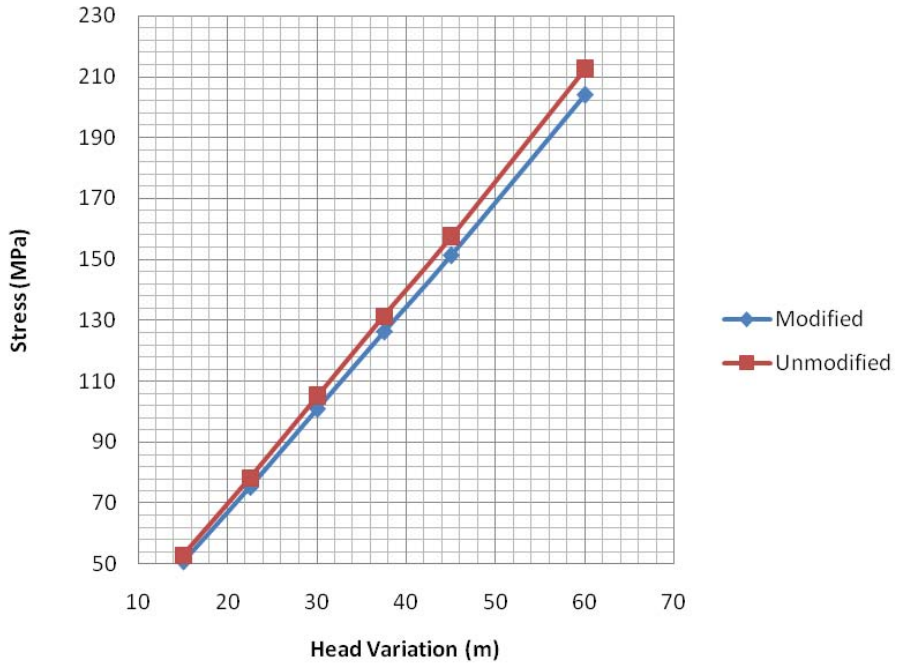

Figure 4.14: Experimental stress vs head variation

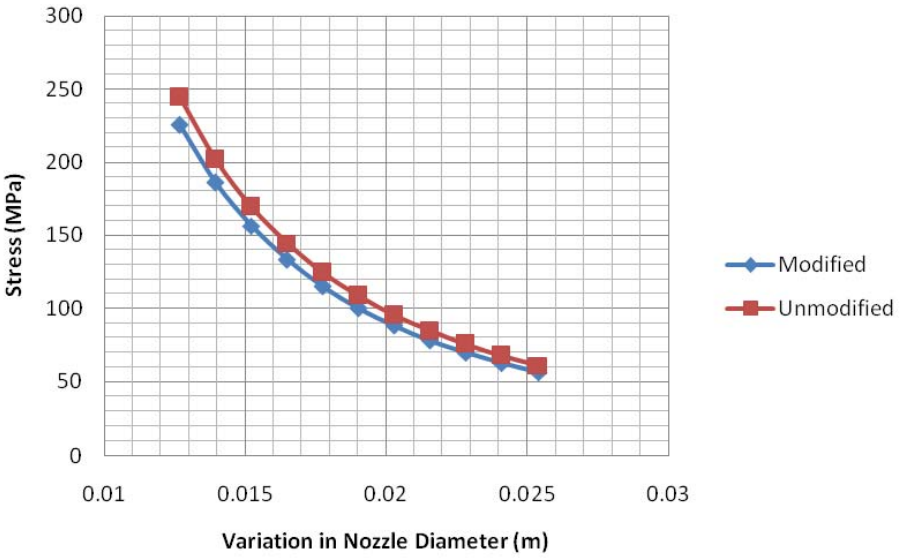

Figure 4.15: Experimental stress vs nozzle diameter variation

plotted as explained in this section.

4.5.1 Relationships Between Head and Stress

In summary Figure 4.16 shows the variation of stress as a results of variation in operation head. It indicates that an increase in head creates more potential energy to run the turbine at accelerated speeds causing more cyclic loading and thus the increase in stress. The figure showes stress variation with head between 15 m and 60 m and corresponding stresses. Increase in head caused a linear increase on stresses on the modified buckets. An optimal head of 40 m was obtained that would produce a stress of about 150 MPa which is within yield strength of the material used to fabricate the buckets.

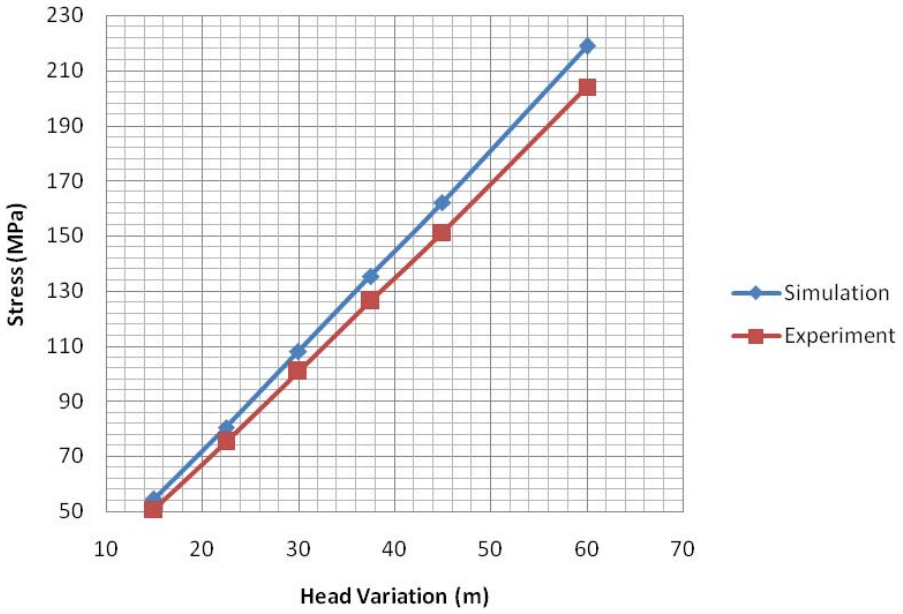

Figure 4.16: Stress vs head variation for modified bucket

4.5.2 Relationships Between Nozzle Diameter and Stress

Figure 4.17 shows stress variation with the charge of nozzle diameter between 0.0127 m and 0.0254 m. As the diameter of the nozzle increase, the stress on the buckets reduces exponentially in the modified buckets. At an optimum operating stress on the buckets of 15 MPa an average nozzle diameter of 0.016 mm was obtained from the graphs.

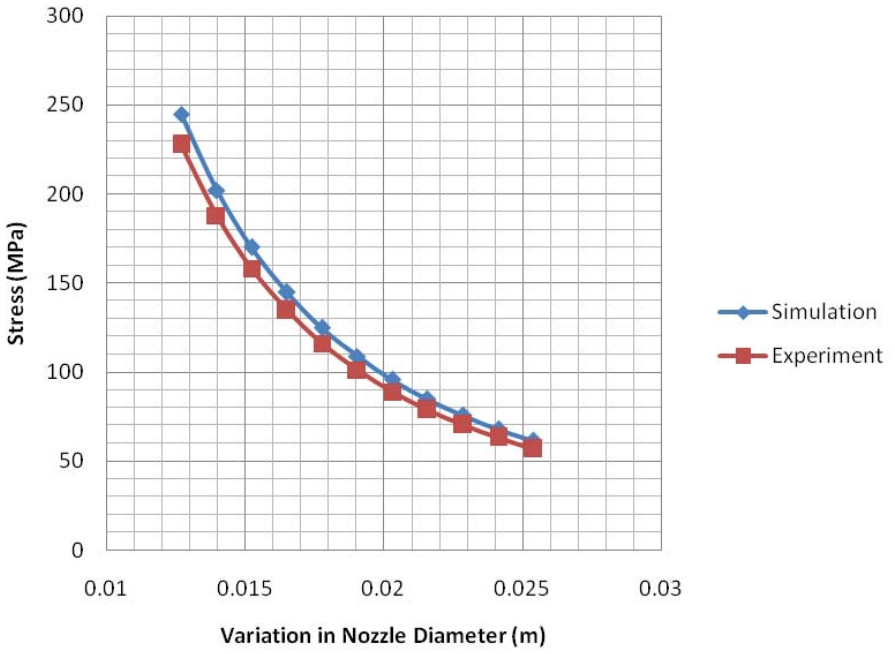

Figure 4.17: Stress vs nozzle diameter variation for modified bucket

CHAPTER FIVE

CONCLUSIONS AND RECOMMENDATIONS

5.1 Conclusions

The research presented modeling and validation of the results experimentally on Pelton buckets made from recycled aluminium that is readily available in Kenyan market. The results showed that by modifying the Pelton bucket profile there was a 14% reduction in stress. The modeling results showed that 152 mm PCD turbine can be operated to produce up to 5 kW within a good safety factor without fear of failure in cyclic loading. Conclusions from the study are as outlined below.

- Experiments conducted verified the modeling results and at equivalent jet loading to produce 5 kW power output the buckets experienced stress of 150 MPa, a value that is below the yielding strength of the recycled aluminium A356. The water jet force that drives the turbine was computed for head variations between 15m and 60m and obtained to be between 275.3 N and 1105.2 N. The water jet force of nozzle diameter variations between 0.0254 m and 0.0127 m was found to be between 309.2 N and 1236.8 N. This were used as the input parameters to calculate the stresses on the buckets and to obtain the optimum operation conditions for a 152 mm PCD Pelton turbine. An optimum nozzle diameter of 0.016 m was found for power output of 5 kW. This will produce enough kinetic energy without causing fatigue failure on the turbine runner.

- The aluminium alloy A356 with a yield strength of 207 MPa was used to produce the turbine runner that operate at the deduced optimum operating conditions of 40 m and with a turbine with a nozzle diameter of 0.016 m to produce a power output of 5 kW at which the operating stress is 150 MPa. This gives a leeway in case of sudden stopping of the turbine that would cause

the operating stress to rise above 150 MPa before reaching the yield strength of the turbine runner material and thus the turbine runner would not breakdown.

- A field survey was carried out on Kathamba community hydro power plant in Kirinyaga district to assess the mechanical challenges on Pelton turbine. This was intended to create confidence in local manufacturers of Pico-hydro turbines thus making electrification in rural areas more feasible. Frequent failure of the Kathamba community hydro Pelton turbine was noted and this was due to excessive cyclic load on the bearings. This was caused by over rated operating conditions in order to meet the power demand of the community. To overcome this there was need to reevaluate the installation head and redesign the nozzle of the turbine. Data obtained from this research will not only be of great help to this community but also other projects experiencing similar challenges.

- Use of CAD/ CAM software helped in production of the bucket with more precise dimensions and material consistency. The use of the software also reduced production time compared to pattern carving from wood.

- Pelton buckets have intricate parts both internal and external and thus casting was the most appropriate method produce the test buckets; this also minimizes other operations such as machining and welding. The test buckets were cast in a single piece which otherwise would require construction in several pieces and frequent assembly if made by other methods. This resulted into a stronger product which exhibits uniform property thus the results obtained were consistent.

- In order to develop energy systems which are economical, environmentally benign with short gestation period, great emphasis needs to be placed on quick development of small hydropower resources. Small and mini hydro potential can provide a solution for the energy problems in remote and hilly areas

where extension of grid system is comparatively uneconomical. The challenge however, is that technologies in small hydro power are not well established. Through this kind of research improvements are possible to extend the range of the existing small hydro technologies, notably to develop affordable and locally available hydro turbines. This was achievable through use of easily available construction materials to develop and test a low cost power packaged system for use in hydro potential developing countries.

The results from the present study will enhance existing knowledge on the performance of recycled aluminium A356 in production of Pelton turbine by casting. This will allow the next generation of Pelton turbines to be designed making use of a combination of empirical know-how from previous experience and an improved physical understanding of the complex Pelton bucket profile.

5.2 Recommendations

The research showed that modification on the Pelton buckets can be used to improve on the power output of the turbine. More optimization could be carried out on other recycled aluminium alloys of higher mechanical strength.

- A Classic 2-Fluid CFD Model computation should be run with a larger number of iterations to reach a complete convergence and precise results. This should also encompass fluid simulation on the backside of the bucket in the modeling which is paramount to determine more accurately the pressure distribution on the backside of the Pelton buckets.

- The main drawback associated with the structural analysis approach used for the simulation of Pelton buckets was the need for refined meshes in the whole domain. This would have meant an increases in the computational cost required to reach satisfactory predictions. More refined mesh simulation and full-scale simulations of the turbine was difficult to achieve in this case since

high specification machine was required. There is need to carry out a full-scale simulation of the Pelton turbine runner in order to obtain more comprehensive results.

- There is need to carry out design optimization using the knowledge of the Pelton parameters which in turn will permit the use of optimum design based on genetic algorithms (Ferrando L. et al., 2006) to shape the bucket surface in order to reach the highest momentum transfer between the flow and the bucket and thus improve the efficiency, while reducing the mixing losses between the adjacent water filaments.

- Further research on aluminium fabricated Pelton turbines could be carried out. Possible areas of further work could be: Combining CFD simulation with structural analysis for more accurate input conditions of the jet force in test rig for measuring the actual jet force to be used for structural analysis.

REFERENCES

Kiplagat J., Wang R. and Li T., (2011). Renewable energy in Kenya: Resource potential and status of exploitation, *Renewable and Sustainable Energy Reviews,* 15(6) pp. 2960-2973.

Yadoo A. and Cruickshank H., The role for low carbon electrification technologies in poverty reduction and climate change strategies. *A focus on renewable energy mini-grids with case studies in Nepal, Peru and Kenya, energy policy,* (42) pp. 591-602, 2012.

Jagdish L., (1975). *Hydraulic Machines.* Metropolitan Book Co. Privet Ltd.

Logan E. and Roy R. (2003). *Handbook of Turbo Machinery.* Marcel Dekker, Inc., New York.

Helmut K. and Sick M., (2008). Thirty years of Numerical Flow Simulation in Hydraulic Turbomachines, *International Journal of Engineering Science and Technology (IJEST)*, pp. 211-229.

Parkinson E., Garcin H., Vulliod G., Zhang Zh., Muggli F., and Casartelli E., Experimental and numerical investigation of the free jet flow in a model nozzle of a Pelton turbine, *tech. rep., Lausanne, Switzerland,* 2007.

Gaurangkumar C., Chaudhari D., Channiwala S. and Samip P., Comparative assessment of the developed stress in both traditional and hooped Pelton runners, *tech. rep., Institutie of Technology, Surat India,* 2005.Kuhlmann H. and Rath J.,(1998). *Free Surface Flows.* Springer publishing, Wien.

Kovalev N., Hydroturbines - Design and Construction, *tech. rep., Mash-iostroite lnoi literatury Moscow-Leningrad,* 1961.

Sick M., Keck H., Parkinson E., and Vullioud G, New Challenges in Pelton Research. *Hydro Conference, Bern, Switzerland,* 2000.

Mack R., Rohne W., Riemann S., Knapp W., and Schilling R., (2006). Using the Potential of CFD for Pelton Turbine Development, *tech. rep., Yokohama, Japan.*

Perrig A., Avellan F., Kueny J., Farhat M., and Parkinson E.,(2006). Flow in a Pelton turbine bucket: Numerical and experimental investigations. *Transactions of the ASME: Journal of Fluids Engineering*, (128): 350-358.

Alexandre P., Franois A., Jean-Louis K., and Mohamed F., (2005). Flow in a Pelton Turbine Bucket: Numerical and Experimental Investigations, *tech. rep., CH-1015 Lausanne, Switzerland.*

Vesely J. and Varner M., (2000 September 27). A Case Study of Upgrading of 625 MW Pelton Turbine, *tech. rep., CKD Blasko Strojirny Czech Republic.* pp. 25.

Bernard M., Georges R., Pierre L. and Pierre Y. L., (2003). Hooped Pelton Runner, *tech. rep., Alstom Power.*

Mayse F.,Pierre Y. and Gerard V., (2002 May 12) Development and Recent Projects for Hooped Pelton Turbine, *tech. rep., Alstom Power.* Pp.12.

Channiwala S. and Gaurang C., Analysis, (2008). Design and Flow Simulation of Advanced Pelton Wheel, *tech. rep., SVNIT, Surat.*

Heinz B., Josef P. and Christian R., Investigation of the Flow in Pelton Turbine and the Influence of the Casing, *tech. rep., Austria.* 1997.

Kvicinsky S., Kueny J. and Avellan F., (2002). Numerical and Experimental Analysis of Free Surface Flows in a 3D Non-Rotating Pelton Bucket. textit The 9th International Symposium on Transport Phenomena and Dynamic Rotating Machinery, Honolulu.

Gilbert G. and Gordon J, (2003). Low cost Pelton turbine design and testing,

tech. rep., Hydroplan UK Gilbert Gilkes Gordon Ltd.

Longatte F., Kvicinsky S., Avellan F. and Jean L., (1999). Free Surface Flows: Experimental Validation of the Volume of Fluid VOF Method in the Plane Wall Case, *Proceedings of 3rd ASME/JSME, San Francisco, ASME, New York,* pp. 18.

Zhang Z. and Casey M.,(2007). Experimental studies of the jet of a Pelton turbine, *Proc. IMechE, Part A: J. Power and Energy,* 221(A8), 1181-1192.

Ciocan G., Liescu M., Vu T., Nennemann B. and Avellan F., (2007). Experimental study and numerical simulation of the flint draft tube rotating vortex. *Journal of Fluids Engineering,* 129(2) pp. 146-158.

Xiao Y., Han F., Zhou J. and Kubota T., (2007). Numerical prediction of dynamic performance of Pelton turbine, *Journal of Hydrodynamics, Ser. B.* 19(3) pp. 356-364.

Brekke H., A general study on the design of vertical Pelton turbine. *Turbo-institute Conference on Hydraulic Machinery,* 1984.

Thake J., (2011) *The Micro-hydro Pelton Turbine Manual.* Practical Action Publishing.

Yury S. Lerner, Nageswara R., (2013). *Metal Casting Principles and Techniques,* (1). American Foundry Society.

Ferrando L. and, Lluis k., (2006). *Surface parameterization and optimum design methodology for hydraulic turbines.* Lausanne, EPFL.

Chepuis L. and Froschl K., (1998). Optimized fabrication of Pelton turbine runners, *Hydropower and Dams Magazine,* 5(2) pp. 30-32.

APPENDICES

Appendix I: Hydro Turbines

Hydro turbines extract energy from water which has a high head. There are basically two types, reaction and impulse, the difference being in the manner of head conversion. They can also be of radial, axial or mixed flow types [**?**]. the section below discusses the different types.

Classification of Hydro Turbines

Hydro turbine are classified based on pressure change withing the turbine runner or based on the flow path the driving water takes within the runner.

Classification Based on Pressure Change

i. Impulse Turbine

In impulse turbines the high head is first converted through a nozzle into a high velocity jet which strikes the blades at one position as they pass by. The pressure of liquid does not change while flowing through the rotor of the machine. Pressure change occurs only in the nozzles of the machine. The high pressure is confined to the small nozzle which converts the head to an atmospheric pressure jet of high velocity. The jet strikes the buckets and imparts a momentum change. One such example of impulse turbine is Pelton wheel. The Pelton turbine in Figure 1 is ideal for this situation.

ii. Reaction Turbine

In reaction turbines the water fills the blade passages and the head change or pressure drop occurs within the impeller. The pressure of liquid changes while it flows through the rotor of the machine. The change in fluid velocity and reduction in its pressure causes a reaction on the turbine blades; this is where from the name Reaction turbine may have been derived. Francis and Kaplan turbines fall in the category of reaction turbines. Reaction turbines

Figure 1: Aluminum Pelton turbine fabricated at JKUAT

are generally low-head, high-flow devices. The flow is opposite to that in a pump (from volute to eye of impeller after transferring most of the energy of the water to the impeller) but a difference is the important role stationary guide vanes play. Purely radial and mixed flow designs are called Francis turbines. At even lower heads an axial flow, propeller turbine is more compact. It can be fixed bladed but better efficiency is obtained over an operating range by using adjustable vanes, in the Kaplan turbine.

Classification of Hydro Turbines Based on Flow Path

i. Axial Flow Hydraulic Turbines

This category of hydraulic turbines has the flow path of the liquid mainly parallel to the axis of rotation. Kaplan Turbines has liquid flow mainly in axial direction.

ii. Radial Flow Hydraulic Turbines

Such Hydraulic Turbines has the liquid flowing mainly in a plane perpendicular to the axis of rotation.

iii. Mixed Flow Hydraulic Turbines

For most of the hydraulic turbines used there is a significant component of both axial and radial flows. Such types of hydraulic turbines are called as Mixed Flow Turbines. Francis turbine is an example of mixed flow type, in Francis turbine water enters in radial direction and exits in axial direction. None of the hydraulic turbines are purely axial flow or purely radial flow. There is always a component of radial flow in axial flow turbines and of axial flow in radial flow turbines.

Pelton Turbine Operating Principle

The bucket has two functions;

i. Transformation of kinetic energy of the jet into a tangential force.

ii. Transmission of the torque generated by this force to the runner rim.

Performance Related Components of a Pelton Turbine

They consist of a distributor/manifold, housing/casing, nozzle/needle jet, impulse runner and discharge chamber/tail race.

i. Distributor/Manifold

The function of the distributor (or manifold) is to provoke an acceleration of the water flow towards each of the main injectors. The advantage of this design is to keep a uniform velocity profile of the flow.

ii. Housing/Casing

The function of the housing is to form a rigid unit with passages for the needle piping, brake mechanisms, and the deflector shafts. The shape of the inner side of the housing is important for directing the exit water effectively away from the runner. It also has the following functions; it prevents accidents, Minimize the wind losses, stops splashing of water,facilitates to collect water, transmission of water to the tail race.

iii. Nozzle/Needle Valve

Nozzle of a Pelton wheel is a circular guide mechanism which guides the water to flow at the desired directions. It also regulate the flow of water. A conical or spear needle operates inside the nozzle in axial direction. The main purpose of the nozzle is to regulate the flow of water through nozzle. When the needle is pushed forward into the nozzle, it reduces area if jet. As a result the quantity of water through the jet is also reduced. Similarly if the spear is pushed back out of nozzle, it increases the area of nozzle and discharge increases.The movement of spear is regulated by hand or by automatic governing arrangement. Sometimes it is very essential to close the nozzle suddenly. It is necessary when there is a sudden decrease of load on turbine. To close the nozzle, if we use spear then it will cause the pipe to burst due to high pressure generation. In order to avoid such a mishap, an additional nozzle is provided through which the water can pass without striking the buckets. This needle is known as bypass needle.Sometimes, a plate known as deflector plate is provided to the nozzle, which is used to deflect water jet.The shape is designed for rapid acceleration at the exit end and for assuring a uniform water jet shape at all openings. The needle valve/nozzle assembly is placed close to the runner as possible to avoid jet dispersion due to air friction (Kovalev N. 1961).

iv. Runner and buckets

Runner of a Pelton wheel consists of circulating disc fixed with horizontal shaft. On the periphery of the runner, a number of buckets are fixed at a uniform distance. Bucket is a hemispherical cup or bowl with a divider in the middle. This divider is known as splitter. It split the water jet in two equal parts. It is turned by forced jets of water which are discharged from one or more nozzles. The resulting impulse spins the turbine runner, imparting energy to the turbine shaft. The surface of the bucket is made very smooth. For low heads, the buckets are made of cast iron. For high heads, buckets are made of stainless

steel, bronze or other alloys. For impure water, buckets are made of special alloys. The buckets are generally bolted to the runner disc. Sometimes the buckets and disc are cast as a single unit. Sometimes few buckets are damaged and need replacement. They can only be replaced if they are bolted with the runner disc.

v. Discharge Chamber/ tail race

The function of the discharge chamber is to enable water existing the runner to fall freely toward the drainage. It also functions as a shield for the concrete work and avoids concrete deteriorations due to the action of the water jets. Correct water level regulation (surge chambers) inside this chamber is critical for maximum efficiency.

Non-performance Related Components of a Pelton Turbine

They include the deflector,braking jet, turbine shaft and guide bearing.

i. Deflectors

The deflectors have the function to bend the jet away from the runner at load rejections to avoid too high of a speed increase. Moreover it protects the jet against exit water spray from the runner. The deflector arc is bolted to the deflector support structure frame with the control valve of the needle servomotors. A seal ring around the deflector shaft bearing housing prevents water and moisture from penetrating into the bearing.

ii. Braking jet

Whenever the turbine has to be brought to rest the nozzle is completely closed. But the runner of Pelton wheel goes on revolving due to inertia. To bring the runner to rest in short time, a small nozzle is provided in such a way that it will direct the jet of water on the back of buckets. It acts as a brake for reducing the speed of the runner.

iii. Turbine Shaft

The function of the turbine shaft is to transfer the torque from the turbine runner to the generator shaft and rotor. The shaft typically has a bearing journal for oil lubricated hydrodynamic guide bearings on the turbine runner end. Shafts are usually manufactured from forged steel, but some of the larger shafts can be fabricated.

iv. Guide Bearing

The function of the turbine guide bearing is to resist the mechanical imbalance and hydraulic side loads from the turbine runner, thereby maintaining the turbine runner in its centered position in the runner seals. It is typically mounted as close as practical to the turbine runner and supported by the head cover. Turbine guide bearings are usually oil lubricated hydrodynamic bearings.

Appendix II: Turbine Parameters

Number of Buckets

An important aspect during turbine design is to consider the number of buckets. The number of buckets for a given runner must be determined so that no water particle is lost while minimizing the risks of detrimental interactions between the out flowing water particles and the adjacent buckets. The runner pitch is determined by the paths of the bucket tip. The bucket pitch must be selected so that no particle stemming from the jet can escape the runner without encountering any bucket (Sick M. et al., 2000).

Bucket Angle of Setting

The splitter is not radially oriented, but inclined towards the jet. The bucket angle of setting is set so that the splitter lies perpendicular to the jet axis when the center of gravity of the jet reaches the bucket (Sick M. et al., 2000). This is an important parameter that will be taken in to account during analysis.

Bucket Surface Profile

To avoid a rapid destruction of the splitter, the splitter angle is usually smaller than 20^o, while the outflow angle is around 10^o. One of the major aspects of the bucket design process is defining the inner surface curves as shown in Figure 2.

Model tests are carried out to assess the validity of the results, and modifications performed if necessary until the final shape is obtained. The cutout area and the bucket backside shapes are designed so that the jet does not impinge on the rear side of the cutout too early (inlet heeling) (Helmut K et al., 2008).

Pelton Turbine Nozzle

The Pelton nozzle converts the pressure energy of the water in the penstock into the kinetic energy of the water jet. Figure 3 shows a typical Pelton nozzle. The water converges within the nozzle and contininue to converge outside the nozzle until the jet reaches a minimum diameter, which is called “Vena Contracta”. At the “Vena

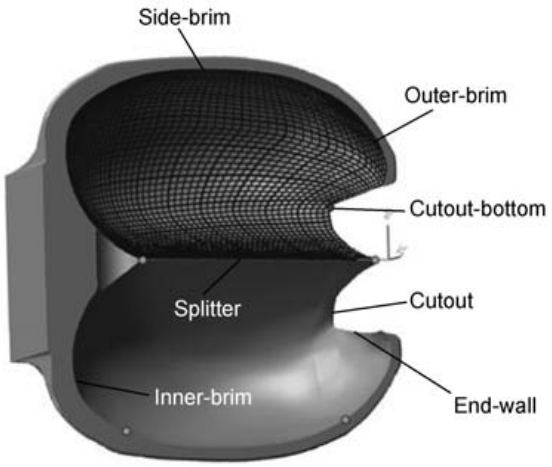

Figure 2: Complicated boundary of a Pelton bucket

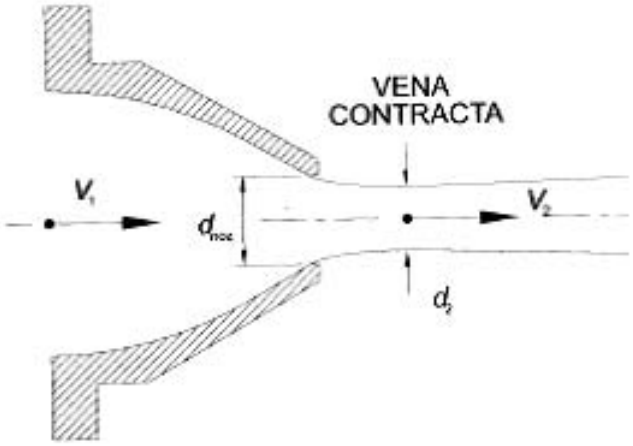

Figure 3: Water jet emerging from a typical nozzle

Contracta" the lines of flow within the jet are parallel. The pressure in the jet does not settle down to atmospheric until the "Vena Contracta", and the velocity of the jet increases slightly between the nozzle and the minimum diameter. After the "Vena Contracta", the jet slowly diverges because of friction between the air and the jet. The velocity of the jet at "Vena Contracta" is given as:

$$V_2 = C_v.\sqrt{2g.H_n} \tag{1}$$

The contraction of the jet down to the "Vena Contracta" is described by a contraction coefficient C_c such that

$$A_2 = C_c.A_{nozzle}$$

The discharge coefficient C_D gives the actual flow from the nozzle;

$$Q = C_D.A_{nozzle}.\sqrt{2g.H_n} \tag{2}$$

Note;

$$C_D = C_c.C_v$$

Relations for Pelton Turbines

In the following some useful relations are listed. Some are needed to evaluate the experimental results.

Alignment and Balancing

The alignment and balancing of a turbine greatly affects its performance and durability. Due to high rotational rates and cyclic forces, small misalignments can cause large negative effects. The most important alignment is that of the splitter ridge of each bucket with the center of the jet. Misalignment here not only causes large losses in efficiency but can also damage the buckets and turbine. With the splitter ridge off center, more of the jet is received by one side, overloading one side of the bucket and inducing stress on its stem. Misalignment has less effect on the wear of the turbine but can reduce the performance. If the water jet nozzle is too far from the turbine, the jet starts to diverge and loses its power before reaching the bucket. If the turbine sits too high or too low with respect to the nozzle, the jet does not contact the buckets correctly resulting in reduced efficiency from either less power transfer or greater interference (Sick M. et al., 2000).

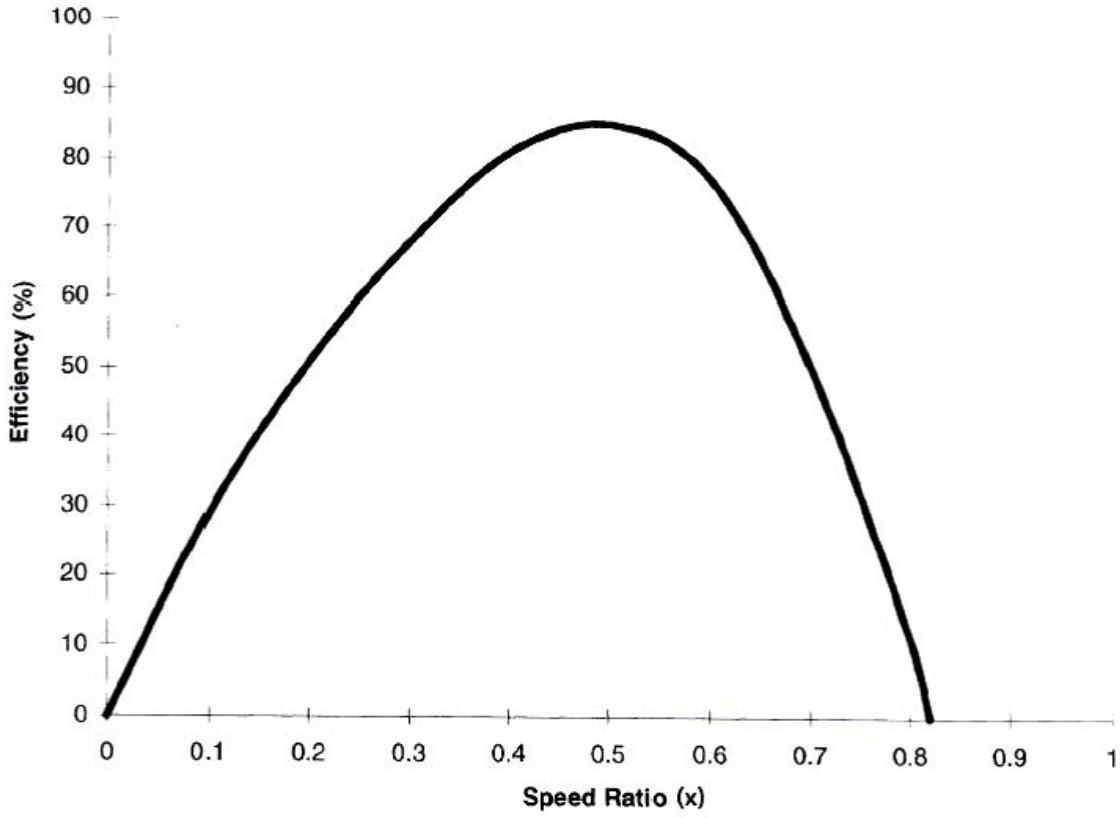

Figure 4: Theoretical Pelton runner turbine efficiency vs. speed ratio

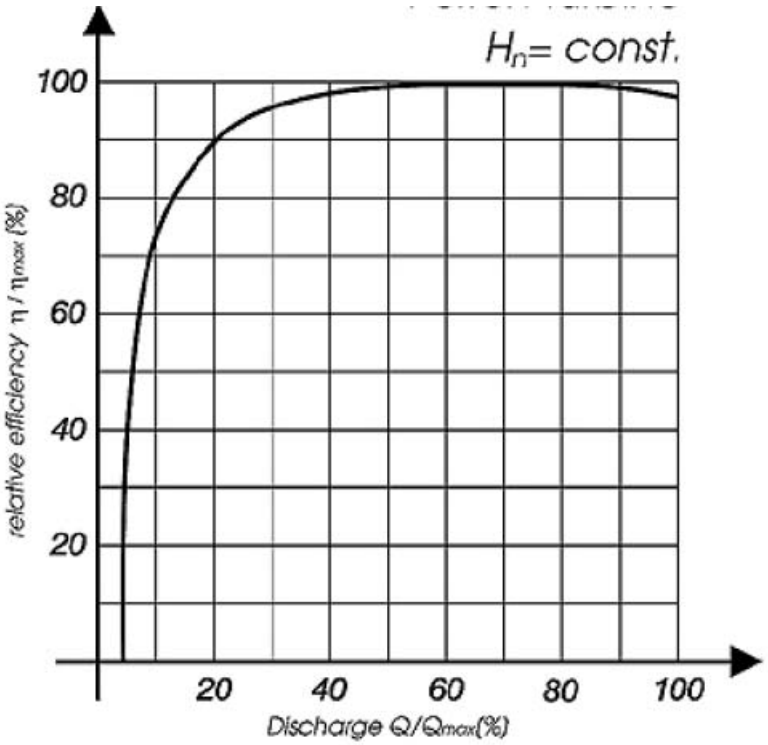

Figure 5: Pelton runner relative efficiency vs rated flow

Appendix III: Derivations

Flow Simulation

The behavior of the flowing fluid inside the Pelton bucket is numerically analyzed using flow governing equations. These include:-

i. The conservation of mass equation.

ii. The momentum conservation equation.

iii. The Bernoulli's Equation.

Conservation of Mass Equation

The total amount of fluid in a controlled volume is conserved.The equation is given as:-

$$\frac{\partial \rho}{\partial t} + \frac{\partial \rho u}{\partial x} + \frac{\partial \rho v}{\partial y} = 0 \tag{3}$$

where;

ρ is density

t is temporal coordinate

x and y are spatial coordinate

u and v are the velocity components in x and y directions respectively

∂ is partial differential operator.

Momentum Conservation Equation

In applying Newton's second law of motion to a finite extended mass of fluid, the external resultant force is equated to the rate of change of resultant momentum which is calculated for a mass of fluid consisting of the same fluid particles.

x momentum conservation

$$\frac{D\rho u}{Dt} = -\frac{\partial \rho}{\partial x} + \rho g_x + \frac{\partial}{\partial x}\mu\left(\frac{2\partial u}{\partial x} - \frac{2}{3}\nabla u\right) + \frac{\partial}{\partial y}\mu\left(\frac{\partial u}{\partial y} + \frac{\partial v}{\partial x}\right) \tag{4}$$

y momentum conservation

$$\frac{D\rho v}{Dt} = -\frac{\partial \rho}{\partial y} + \rho g_y + \frac{\partial}{\partial y}\mu\left(\frac{2\partial v}{\partial y} - \frac{2}{3}\nabla u\right) + \frac{\partial}{\partial x}\mu\left(\frac{\partial u}{\partial y} + \frac{\partial v}{\partial x}\right) \tag{5}$$

where

$$\nabla u = \frac{\partial u}{\partial x} + \frac{\partial v}{\partial y} \tag{6}$$

is gradient operator

$$\frac{D}{Dt} = \frac{\partial}{\partial t} + \frac{\partial u}{\partial x} + \frac{\partial v}{\partial y} \tag{7}$$

is cumulative and convective operator

ρ is the density

μ is dynamic viscosity

g is gravitational acceleration

x and y are spatial coordinate

u and v are the velocity components in x and y directions respectively

Bernoulli's Equation

The power output of an ideal turbine PT is derived from (a simplified) BERNOULLI's equation with the following assumptions:

i. No friction

ii. No viscosity

iii. Incompressible medium

iv. Laminar flow

v. Steady flow

The only parameters that have to be taken into account are the pressure and velocity differences at inlet and outlet of the turbine.

$$P_T = \left(\frac{p_1 - p_2}{\rho} + \frac{c_1^2 - c_2^2}{2} \right) . \frac{dm}{dt} \tag{8}$$

where

$$\frac{p_1 - p_2}{\rho}$$

stands for the specific potential energy of the water flow, whereas

$$\frac{c_1^2 - c_2^2}{2}$$

denotes the specific kinetic energy. Thus the expression

$$P_T = \left(\frac{c_1^2 - c_2^2}{2} \right) . \frac{dm}{dt}$$

describes the net power output of an ideal impulse turbine, where all potential energy is transformed into velocity (i.e. kinetic) energy.

Impulse Forces

Impulse (i.e momentum) is defined as product of velocity and mass $j = mv$, thus being a quantity of motion. The pulse force is defined as the first derivative of the momentum:

$$\frac{d\,(m.v)}{dt} = \frac{dj}{dt} = F \tag{9}$$

In a closed system the sum of all acting forces equals zero, thus the forces of deflection, acceleration (positive or negative) are in equilibrium with the pulse force(s). The runner of the turbine is driven by the negative acceleration of the peripheral flow of the jet, with flow velocity c_1. The product of torque M_T and the rotational speed of the turbine, which equals the power output P_T , can be related to the flow

rate

$$Q = \frac{1}{\rho}.\frac{dm}{dt} \tag{10}$$

and the periphal velocity u of the runner by means of:

$$P_T = M_T.\omega = \rho.Q.\left(c_1 - c_2\right).u \tag{11}$$

with c_1 and c_2 the velocity components of the jet in the direction of u before and after touching the bucket. The efficiency of the turbine η is given by the ratio of the power output at the turbine shaft P_T and the kinetic power P_{jet} of the water jet. This leads to a general equation for the turbine efficiency:

$$\eta = \frac{P_T}{Pjet} = \frac{\rho.Q.\left(c_1 - c_2\right).u}{\frac{1}{2}.\rho.Q.c_1^2} \tag{12}$$

and then a variable k

$$k = \frac{u}{c_1}$$

is defined, which gives the ratio between the periphal velocity of the runner u and the linear velocity of the jet c_1 (before hitting the runner). The optimal rotational speed ω_{opt} can be calculated from the first derivative of the efficiency over k:

$$\frac{d\rho}{dk} = 0\left(\omega = \omega_{opt}\right) \tag{13}$$

and the solutions for the Pelton turbine are given below.

Structural Analysis Fundamentals

The following two topics on structural fundamentals were applied in ANSYS software to carry out the static structural analysis:

i. Stress-Strain Relationships.

ii. Temperature-Dependent Coefficient of Thermal Expansion.

Stress-Strain Relationships

This section discusses material relationships for linear materials given that the aluminum alloy that was used to cast the Pelton buckets is a linear material. The stress is related to the strains by:

$$\{\sigma\} = [D]\left\{\epsilon^{el}\right\} \tag{14}$$

where;

σ is stress vector = $\lfloor \sigma_x \quad \sigma_y \quad \sigma_z \quad \sigma_{xy} \quad \sigma_{yz} \quad \sigma_{xz} \rfloor^T$

$[D]$ is elasticity or elastic stiffness matrix or stress-strain matrix (defined in Equation through) or inverse defined in Equation

$\left\{\epsilon^{el}\right\}$= $\{\epsilon\}$ - $\left\{\epsilon^{th}\right\}$ which is elastic strain vector

$\{\epsilon\}$ is total strain vector = $\lfloor \epsilon_x \quad \epsilon_y \quad \epsilon_z \quad \epsilon_{xy} \quad \epsilon_{yz} \quad \epsilon_{xz} \rfloor^T$

$\left\{\epsilon^{th}\right\}$ = thermal strain vector defined by Equation

Note:

The $\left\{\epsilon^{el}\right\}$ are the strains that cause stresses.

The shear stains ($\epsilon_{xy} \quad \epsilon_{yz} \quad \epsilon_{xz}$) are the engineering shear strains, which are twice the tensor shear stains.

The ϵ notation is commonly used for tensor shear strains, but is used here as engineering shear stains for simplicity of output.

The stress vector is shown in the Figure 6 below. The sign convention for direct stresses and strains used throughout the ANSYS program is that tension is positive and compression is negative. For shears, positive is when the two applicable positive axes rotate toward each other.

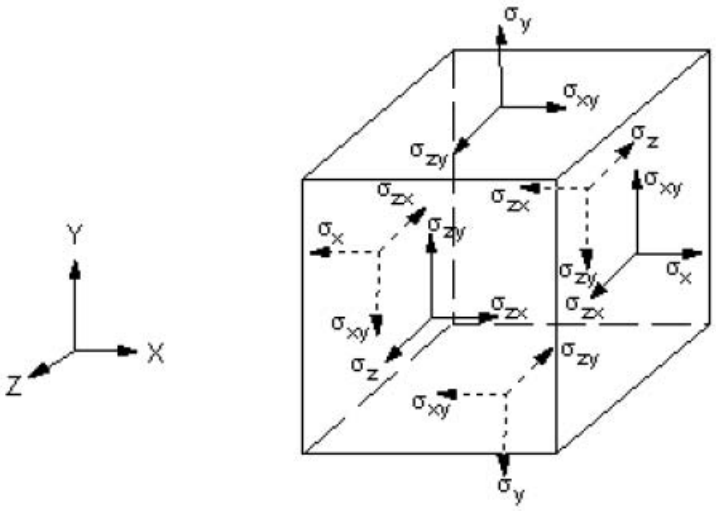

Figure 6: Stress vector definition

Equition 14 may also be inverted to:

$$\{\epsilon\} = \left\{\epsilon^{th}\right\} + [D]^{-1}\{\sigma\} \tag{15}$$

For the 3-D case, the thermal strain vector is:

$$\left\{\epsilon^{th}\right\} = \Delta T \left\lfloor \alpha_x^{se} \quad \alpha_y^{se} \quad \alpha_z^{se} \quad 0 \quad 0 \quad 0 \right\rfloor^T \tag{16}$$

Where;

α_x^{se} is secant coefficient of thermal expansion in the x direction

$$\Delta T = T - T_{ref} \tag{17}$$

T is current temperature at the point in question

T_{ref} is reference (strain-free) temperature

The flexibility or compliance matrix, $[D]^{-1}$ is:

$$[D]^{-1} = \begin{bmatrix} 1/E_x & -\upsilon_{xy}/E_x & -\upsilon_{xz}/E_x & 0 & 0 & 0 \\ -\upsilon_{yx}/E_y & 1/E_y & -\upsilon_{yz}/E_y & 0 & 0 & 0 \\ -\upsilon_{zx}/E_z & -\upsilon_{zy}/E_z & 1/E_z & 0 & 0 & 0 \\ 0 & 0 & 0 & 1/G_{xy} & 0 & 0 \\ 0 & 0 & 0 & 0 & 1/G_{xy} & 0 \\ 0 & 0 & 0 & 0 & 0 & 1/G_{xy} \end{bmatrix} \tag{18}$$

where typical terms are;

E_x is Young's modulus in the x direction

υ_{xy} is Major Poisson's ratio

υ_{yx} is Minor Poisson's ratio

G_{xy} is shear modulus in the xy plane

Also the $[D]^{-1}$ matrix is presumed to be symmetric, so that:

$$\frac{\upsilon_{yx}}{E_y} = \frac{\upsilon_{xy}}{E_x} \tag{19}$$

$$\frac{\upsilon_{zx}}{E_z} = \frac{\upsilon_{xz}}{E_x} \tag{20}$$

$$\frac{\upsilon_{zy}}{E_z} = \frac{\upsilon_{yz}}{E_y} \tag{21}$$

Expanding Equation 15 with Equation 16 we get the six explicit Equations:

$$\epsilon_x = \alpha_x \Delta T + \frac{\sigma_x}{E_x} - \frac{\upsilon_{xy}\sigma_y}{E_x} - \frac{\upsilon_{xz}\sigma_z}{E_x} \tag{22}$$

$$\epsilon_y = \alpha_y \Delta T - \frac{\upsilon_{xy}\sigma_x}{E_x} + \frac{\sigma_y}{E_y} - \frac{\upsilon_{yz}\sigma_z}{E_y} \tag{23}$$

$$\epsilon_z = \alpha_z \Delta T - \frac{\upsilon_{xz}\sigma_x}{E_x} - \frac{\upsilon_{yz}\sigma_y}{E_y} + \frac{\sigma_z}{E_z} \tag{24}$$

$$\epsilon_{xy} = \frac{\sigma_{xy}}{G_{xy}} \tag{25}$$

$$\epsilon_{yz} = \frac{\sigma_{yz}}{G_{yz}} \tag{26}$$

$$\epsilon_{xz} = \frac{\sigma_{xz}}{G_{xz}} \tag{27}$$

Where;

ϵ_x is direct strain in the x direction

σ_x is direct stress in the x direction

ϵ_{xy} is shear strain in th x-y plane

σ_{xy} is shear stress on the x-y plane

Alternatively, Equation 14 may be expanded by first inverting Equation 18 and then combining that result with Equation 16 and Eqution 19 through Equation 21 to give six explicit equations:

$$\begin{aligned}\sigma_x =& \frac{E_x}{h}\left(1 - (\upsilon_{yz})^2 \frac{E_z}{E_y}\right)(\epsilon x - \alpha_x \Delta T) + \frac{E_y}{h}\left(\upsilon_{xy} + \upsilon_{xz}\upsilon_{yz}\frac{E_z}{E_y}\right)(\epsilon_y - \alpha_y \Delta T) \\ &+ \frac{E_z}{h}\left(\upsilon_{xz} + \upsilon_{yz}\upsilon_{xy}\right)(\epsilon_z - \alpha_z \Delta T)\end{aligned} \tag{28}$$

$$\begin{aligned}\sigma_y =& \frac{E_y}{h}\left(\upsilon_{xy} + \upsilon_{xz}\upsilon_{yz}\frac{E_z}{E_y}\right)(\epsilon x - \alpha_x \Delta T) + \frac{E_y}{h}\left(1 - (\upsilon_{xz})^2 \frac{E_z}{E_x}\right)(\epsilon_y - \alpha_y \Delta T) \\ &+ \frac{E_z}{h}\left(\upsilon_{yz} + \upsilon_{xz}\upsilon_{xy}\frac{E_y}{E_x}\right)(\epsilon_z - \alpha_z \Delta T)\end{aligned} \tag{29}$$

$$\begin{aligned}\sigma_z =& \frac{E_z}{h}\left(\upsilon_{xz}+\upsilon_{yz}\upsilon_{xy}\right)\left(\epsilon x-\alpha_x\Delta T\right)+\frac{E_z}{h}\left(\upsilon_{yz}+\upsilon_{xz}\upsilon_{xy}\frac{E_y}{E_x}\right)\left(\epsilon_y-\alpha_y\Delta T\right)\\ &+\frac{E_z}{h}\left(1-\left(\upsilon_{xy}\right)^2\frac{E_y}{E_x}\right)\left(\epsilon_z-\alpha_z\Delta T\right)\end{aligned} \tag{30}$$

$$\sigma_{xy}=G_{xy}\epsilon_{xy} \tag{31}$$

$$\sigma_{yz}=G_{yz}\epsilon_{yz} \tag{32}$$

$$\sigma_{xz}=G_{xz}\epsilon_{xz} \tag{33}$$

Where;

$$h=1-\left(\upsilon_{yx}\right)^2\frac{E_y}{E_x}-\left(\upsilon_{yz}\right)^2\frac{E_z}{E_y}-\left(\upsilon_{xz}\right)^2\frac{E_z}{E_x}-2\upsilon_{xy}\upsilon_{yz}\upsilon_{xz}\frac{E_z}{E_x} \tag{34}$$

Since G_{xy},G_{yz} and G_{xz} were not for isotropic matrerials, they were computed as:

$$G_{xy}=G_{yz}=G_{xz}=\frac{E_x}{2\left(1+\upsilon_{xy}\right)} \tag{35}$$